AMERICAN JOURNAL OF PHYSIOLOGY
REGULATORY, INTEGRATIVE AND COMPARATIVE PHYSIOLOGY

Am J Physiol Regul Integr Comp Physiol 321: R655–R671, 2021.
First published September 8, 2021; doi:10.1152/ajpregu.00175.2021

RESEARCH ARTICLE

Adrenergically induced translocation of red blood cell β-adrenergic sodium-proton exchangers has ecological relevance for hypoxic and hypercapnic white seabass

Till S. Harter, Alexander M. Clifford, and Martin Tresguerres

Marine Biology Research Division, Scripps Institution of Oceanography, University of California San Diego, La Jolla, California

Abstract

White seabass (*Atractoscion nobilis*) increasingly experience periods of low oxygen (O_2; hypoxia) and high carbon dioxide (CO_2, hypercapnia) due to climate change and eutrophication of the coastal waters of California. Hemoglobin (Hb) is the principal O_2 carrier in the blood and in many teleost fishes Hb-O_2 binding is compromised at low pH; however, the red blood cells (RBC) of some species regulate intracellular pH with adrenergically stimulated sodium-proton-exchangers (β-NHEs). We hypothesized that RBC β-NHEs in white seabass are an important mechanism that can protect the blood O_2-carrying capacity during hypoxia and hypercapnia. We determined the O_2-binding characteristics of white seabass blood, the cellular and subcellular response of RBCs to adrenergic stimulation, and quantified the protective effect of β-NHE activity on Hb-O_2 saturation. White seabass had typical teleost Hb characteristics, with a moderate O_2 affinity (P_{O_2} at half-saturation; P_{50} 2.9 kPa) that was highly pH-sensitive (Bohr coefficient −0.92; Root effect 52%). Novel findings from super-resolution microscopy revealed β-NHE protein in vesicle-like structures and its translocation into the membrane after adrenergic stimulation. Microscopy data were corroborated by molecular and phylogenetic results and a functional characterization of β-NHE activity. The activation of RBC β-NHEs increased Hb-O_2 saturation by ∼8% in normoxic hypercapnia and by up to ∼20% in hypoxic normocapnia. Our results provide novel insight into the cellular mechanism of adrenergic RBC stimulation within an ecologically relevant context. β-NHE activity in white seabass has great potential to protect arterial O_2 transport during hypoxia and hypercapnia but is less effective during combinations of these stressors.

Bohr effect; fish; β-NHE; red tide; Slc9a1b

INTRODUCTION

White seabass (*Atractoscion nobilis*), a teleost fish species endemic to the coastal waters of California, are apex predators with ecological significance, sought-after targets of recreational and commercial fisheries and are gaining importance in aquaculture. Their natural habitat along the kelp forests of the northeastern Pacific is subject to strong seasonal fluctuations in water chemistry, due to the upwelling of deeper waters that are often depleted of oxygen (O_2; hypoxia), have a high carbon dioxide tension (CO_2; hypercapnia) and thus, a low pH (1). In addition, a steadily warming climate and growing anthropogenic nutrient loading are increasing the frequency of large algae blooms ("red tides") in California's coastal waters (2). When these algae blooms wane, the microbial decomposition of their biomass consumes O_2 and produces CO_2 and other toxic and acidic byproducts of biological decay, such as hydrogen sulfide, altogether creating large hypoxic and hypercapnic zones (3). Species that are highly mobile may avoid these areas, but for many sedentary species, survival will depend on enduring these conditions. Climate change at large is steadily creating more hypoxic and acidic oceans and, over generations, some species may adapt to cope with their altered habitats (4). However, the reoccurrence of upwelling and severe algae blooms may acutely expose animals to conditions that far exceed worst-case predictions for the end of the century, creating strong selective pressures for hypoxia and hypercapnia tolerance and perhaps overwhelming the rates at which some species can adapt to climate change.

The most recent severe red tide in Southern California occurred in April-May of 2020, when the water measurements at the pier of the Scripps Institution of Oceanography (SIO) in La Jolla, CA revealed average daily dissolved O_2 levels of <2 mg·L^{-1} and pH as low as 7.06 (normal values are ∼8 mg·L^{-1} O_2 at pH 8.2) (5). At a water temperature of 17°C and 35 ppt salinity, these values correspond to 5.3 kPa P_{O_2} (6) and 1.16 kPa P_{CO_2} (7). Equally alarming was the prolonged duration of hypoxia, where for nine consecutive days water P_{O_2} was below the threshold (4.6 mg·L^{-1}) that is considered lethal for 90% of marine life (8). The SIO aquatics facility is supplied with water taken in at the pier, which resulted in hypoxic and hypercapnic exposures of all research animals, despite every effort to aerate the tanks. However unfortunate, this natural experiment revealed a remarkable tolerance of

Correspondence: T. S. Harter (tharter@ucsd.edu); M. Tresguerres (mtresguerres@ucsd.edu).
Submitted 12 July 2021 / Revised 23 August 2021 / Accepted 6 September 2021

white seabass to these adverse water conditions, despite being deprived the behavioral avoidance of hypoxia that may be recruited in the wild. Therefore, the aim of the present study was to explore the O_2-transport capacity of white seabass with a focus on the cellular mechanisms at the level of the red blood cell (RBC) that may contribute to their hypoxia and hypercapnia tolerance.

For obligate aerobic animals, the challenge to surviving unavoidable environmental hypoxia is balancing the uptake and delivery of O_2 with its consumption in the mitochondria (9). Hemoglobin (Hb) is the principal O_2 carrier in the blood and therefore the cardiovascular O_2-carrying capacity is largely determined by the O_2-binding characteristics of Hb. As such, a higher Hb-O_2 affinity will favor the extraction of O_2 from hypoxic waters and thus, a lower Hb P_{50} (the partial pressure of O_2 at which Hb is 50% saturated) is typically associated with hypoxia tolerance in fishes (10, 11); however, whether white seabass have high-affinity Hbs that would confer some hypoxia tolerance is currently unknown.

Hb-O_2 binding in teleost fishes is highly pH sensitive, where a reduction in pH decreases Hb-O_2 affinity via the Bohr effect (12), and the Root effect prevents Hb from becoming fully O_2-saturated at low pH, even at super-atmospheric P_{O_2} (13, 14). The reduction in Hb-O_2-carrying capacity due to the Root effect is physiologically significant, as it enhances the unloading of O_2 at the eyes and the swim bladder of teleosts, where blood is acidified locally (15–17). In contrast, during a systemic blood acidosis that may occur during exercise or hypoxia, the pH-sensitive Hbs of teleosts may fail to become fully oxygenated at the gills, decreasing the O_2-carrying capacity of arterial blood and leading to hypoxemia at the tissues. Thus, a combined hypoxic and hypercapnic exposure may be especially dangerous for teleosts, as a reduced availability of O_2 in the environment is paired with the simultaneous reduction of Hb-O_2 affinity via the Bohr effect at low pH; however, whether white seabass have highly pH-sensitive Hbs is currently unknown.

Hb is housed within RBCs that, in teleosts, may prevent systemic hypoxemia by actively regulating their intracellular pH (pH_i) to protect Hb-O_2 binding during a reduction in extracellular pH (pH_e). In brief, a decrease in arterial P_{O_2} or pH leads to the release of catecholamines into the blood (18, 19), which bind to a β-adrenergic receptor on the RBC membrane and activate a sodium-proton-exchanger (β-NHE, Slc9a1b,) via the cAMP pathway (20). The extrusion of H^+ by the β-NHE raises pH_i above the equilibrium condition, which increases Hb-O_2 affinity and will promote the extraction of O_2 from hypoxic waters (21). The adrenergic stimulation of RBCs also causes an influx of Na^+ and Cl^- that leads to osmotic swelling and that has been used as a marker to determine the presence of RBC β-NHEs in fish species (22, 23). A broader phylogenetic analysis indicates that most teleosts, but not other fishes, have RBC β-NHEs (24); however, whether white seabass RBCs have β-NHE activity has not been determined.

Based on these considerations, we hypothesized that β-NHE activity in white seabass is an important mechanism that can protect the blood O_2-carrying capacity during environmentally relevant levels of hypoxia and hypercapnia ($P_{O_2} < 5.3$ kPa and $P_{CO_2} < 1.16$ kPa; as observed during red tides). We tested this hypothesis in a series of in vitro experiments and predicted that: *1*) white seabass have a high Hb-O_2 affinity to maintain O_2 uptake under hypoxic conditions, which was addressed by generating oxygen equilibrium curves (OEC) over a range of P_{O_2}; *2*) white seabass display the large Bohr and Root effects that are typical of teleosts, which was addressed by generating OECs over a range of P_{CO_2}, and measuring pH_e and RBC pH_i; *3*) white seabass have a RBC β-NHE, which was addressed using molecular, bioinformatic, and immunocytochemical techniques to establish its presence and localization, and by measuring RBC swelling after adrenergic stimulation and the inhibition of NHEs with amiloride; and finally *4*) the β-NHE response of white seabass would provide a significant protection of blood O_2-carrying capacity under environmentally relevant conditions of normoxic and hypoxic hypercapnia.

MATERIALS AND METHODS

Animals and Husbandry

White seabass (*A. nobilis*, Ayres 1860) were obtained from the Hubbs Sea World Research Institute (HSWRI, Carlsbad) and were held indoors at the SIO aquatics facility for several months before experiments. Photoperiod was set to a 12:12-h light-dark cycle and fish were housed in large fiberglass tanks (~3.5–10 m^3) supplied with flow-through seawater from an inshore intake; the average water temperature at the time of experiments was 17°C. Aeration was provided to ensure normoxic conditions in all tanks (>90% air saturation of O_2) and these water parameters were monitored every day. All fish were fed twice a week with commercial dry pellets (Skretting; Classic Bass 9.5 mm; Stavanger, Norway), and feeding was suspended 48 h before blood sampling. The white seabass used for the determination of blood O_2-binding characteristics had an average weight of 1,146 ± 96 g (n = 8), whereas those used for the β-NHE experiments had an average weight of 357 ± 27 g (n = 6); no fish used in this study experienced the adverse water conditions during red tide events. Animal husbandry and all experimental procedures were in strict compliance with the guidelines by the Institutional Animal Care and Use Committee (IACUC) and approved by the Animal Care Program at the University of California San Diego (Protocol No. S10320).

Blood Sampling

White seabass were individually transferred into darkened boxes supplied with air and flow-through seawater, 24 h before blood sampling. The next day the water supply was shut off and the fish were anesthetized by carefully pouring a diluted benzocaine solution (Fisher Scientific, Acros 150785000; Waltham; concentrated stock made up in ethanol) into the box without disturbing the fish, for a final concentrations of 70 $mg \cdot L^{-1}$ benzocaine (<0.001% ethanol). After visible loss of equilibrium, fish were transferred to a surgery table and positioned ventral-side-up, and their gills were perfused with water containing a maintenance dose of anesthetic (30 $mg \cdot L^{-1}$ benzocaine). Blood sampling was by caudal puncture, and 3 mL of blood were collected into a heparinized syringe. This procedure ensured minimal disturbance of the fish (25), which can decrease blood pH due to air exposure (respiratory acidosis) and due to anaerobic

muscle contractions during struggling (metabolic acidosis). After sampling was completed, the fish were recovered and returned to their holding tank, and each individual was only sampled once. In the laboratory, the blood was centrifuged at 500 *g* for 3 min to separate the plasma from the blood cells. The plasma was collected in a bullet tube and stored overnight at 4°C. To remove any catecholamines released during sampling, the blood cells were rinsed three times in cold Cortland's saline (in mM: NaCl 147, KCl 5.1, CaCl 1.6, $MgSO_4$ 0.9, $NaHCO_3$ 11.9, NaH_2PO_4 3, glucose 5.6; adjusted to the measured plasma characteristics in white seabass of 345 mosmol and pH 7.8), and the buffy coat was aspirated generously to remove white blood cells and platelets. Finally, to allow the RBCs to return to an unstimulated state, the pellet was resuspended in 10 volumes of fresh saline and was stored aerobically on a tilt-shaker, overnight, at 17°C (26).

Blood O_2-Binding Characteristics

The next day, RBCs were rinsed with saline three times and resuspended in their native plasma at a hematocrit (Hct) of 5%; this value was chosen based on preliminary trials and yields an optic density that allows for spectrophotometric measurements of Hb-O_2 binding characteristics (~0.6 mM Hb). A volume of 1.4 mL of blood was loaded into a glass tonometer at 17°C and equilibrated to arterial gas tensions (21 kPa P_{O_2}, 0.3 kPa P_{CO_2} in N_2) from a custom-mixed gas cylinder (Praxair; Danbury). After 1 h, 2 μL of blood were removed from the tonometer and loaded into the diffusion chamber of a spectrophotometric blood analyzer (BOBS, Loligo Systems; Viborg, Denmark). The samples were equilibrated to increasing P_{O_2} tensions (0.5, 1, 2, 4, 8, 16, and 21 kPa P_{O_2}) from a gas mixing system (GMS, Loligo), in 2-min equilibration steps and the absorbance was recorded once every second at 190–885 nm. At the beginning and end of each run, the sample was equilibrated to high (99.7 kPa P_{O_2}, 0.3 kPa P_{CO_2} in N_2 for 8 min) and low (0 kPa P_{O_2}, 0.3 kPa P_{CO_2} in N_2 for 8 min) P_{O_2} conditions; for the calculation of Hb-O_2 saturation from raw absorbance values, it was assumed that Hb was fully oxygenated or deoxygenated under the two conditions, which was confirmed by inspecting the absorption spectra (all raw data are deposited online). A P_{CO_2} of 0.3 kPa was maintained throughout these trials to prevent RBC pH_i from increasing above physiologically relevant levels, and this value was chosen to match that measured in the arterial blood of rainbow trout (*Oncorhynchus mykiss*) in vivo (27). All custom gas mixtures were validated by measuring P_{O_2} with an FC-2 Oxzilla and P_{CO_2} with a CA-10 CO_2 analyzer (Sable Systems, North Las Vegas, NV) that were calibrated daily against high purity N_2, air, or 5% CO_2 in air (Praxair).

An additional 250 μL of blood were removed from the tonometer to measure blood parameters as follows. Hematocrit (Hct) was measured in triplicate in microcapillary tubes (Drummond Microcaps, 15 μL; Parkway), after being centrifuged at 10,000 *g* for 3 min. [Hb] was measured in triplicate using the cyano-methemoglobin method (Sigma-Aldrich Drabkin's D5941; St. Louis, MO) and an extinction coefficient of 10.99 $mmol \cdot cm^{-1}$ (28). Blood pH was measured with a thermostatted microcapillary electrode at 17°C (Fisher Accumet 13-620-850; Hampton; with Denver Instruments UB-10 meter; Bohemia), calibrated daily against precision pH buffers (Radiometer S11M007, S1M004 and S11M002; Copenhagen, Denmark). Thereafter, the blood was centrifuged to separate plasma and RBCs and total CO_2 content (TCO_2) of the plasma was measured in triplicate with a Corning 965 (Midland). The RBCs in the pellet were lysed by three freeze-thaw cycles in liquid nitrogen, and pH_i was measured in the lysate as described for pH_e (29). After these measurements were completed, the P_{CO_2} in the tonometer was increased in steps from 0.3 to 2.5 kPa and, each time, OECs and blood parameters were measured as described.

RBC Swelling after β-Adrenergic Stimulation

After storage of blood samples overnight in saline, the RBCs were rinsed three times in fresh saline and resuspended in their native plasma at a Hct of 25%. A volume of 1.8 mL was loaded into a tonometer and equilibrated to 3 kPa P_{O_2} and 1 kPa P_{CO_2} in N_2 at 17°C for 1 h; similar hypoxic and acidotic conditions have been shown to promote β-NHE activity in other teleost species (30, 31). After 1 h, an initial subsample of blood was taken and Hct, [Hb], pH_e, and pH_i were measured as described previously. Thereafter, the blood was split into aliquots of 600 μL that were loaded into individual tonometers and treated with either of the following: *1*) a carrier control (0.25% dimethyl sulfoxide, DMSO; VWR BDH 1115; Radnor), *2*) the β-adrenergic agonist isoproterenol (ISO; Sigma I6504; 10 μM final concentration, which stimulates maximal β-NHE activity in rainbow trout) (19), or *3*) ISO plus the NHE inhibitor amiloride (ISO + Am; Sigma A7410; 1 mM, according to Ref. 32). These treatments were staggered so that samples from each tonometer could be taken for the measurements of blood parameters at 10, 30, and 60 min after drug additions.

For microscopy, subsamples of blood were taken from individual tonometers at the initial and 60 min time points. A volume of 60 μL was immediately resuspended in 1.5 mL ice-cold fixative (3% paraformaldehyde, 0.175% glutaraldehyde in 0.6× phosphate-buffered saline with 0.05 M sodium cacodylate buffer; made up from Electron Microscopy Sciences RT15949, Hatfield) and incubated for 60 min on a revolver rotator at 4°C. After fixation, cells were washed three times in 1× phosphate-buffered saline (PBS, Corning 46-013-CM, Corning) and stored at 4°C for processing. RBC swelling was visually assessed by differential interference contrast (DIC) with a ×60 objective on a Zeiss Observer Z1 microscope (Oberkochen, Germany). For Western blotting, an additional subsample of 100 μL was removed from the tonometers and centrifuged to remove the saline. The RBC pellet was resuspended in 5 volumes of lysis buffer containing 1 mM DL-dithiothreitol (DTT; Thermo Fisher R0861; Waltham, MA), 1 mM phenylmethylsulfonyl fluoride (PMSF; Sigma P7626), and 10 mM benzamidine hydrochloride hydrate (BHH; Sigma B6506) in PBS. The RBCs were lysed by three cycles of freeze thawing in liquid nitrogen, the lysate was centrifuged at 500 *g* for 10 min at 4°C, and the supernatant was stored at −80°C.

Hb-O_2 Binding after β-Adrenergic Stimulation

An additional aliquot of RBCs was resuspended in native plasma at a Hct of 5%. Volumes of 300 μL were loaded into one of four tonometers and equilibrated to arterial gas

tensions at 17°C (as described previously) and treated with either of the following: *1*) a carrier control (DMSO; 0.25%), *2*) ISO (10 μM), or *3*) ISO + Am (1 mM). These treatments were staggered to allow for standardized measurements at 60 min after drug additions, when 2 μL of blood were removed from the tonometer and loaded into the BOBS for real-time measurements of Hb-O_2 saturation during a respiratory acidosis. Therefore, the blood was exposed to stepwise increases in P_{CO_2} (0.3, 0.5, 1, 1.5, 2, and 3 kPa) allowing for two minutes of equilibration at each step; preliminary trials showed full equilibration to the new P_{CO_2} after ~1 min and absorbance remained constant thereafter. As described previously, this protocol also included initial and final calibration steps, at which the sample was fully O_2 saturated and then desaturated. A first trial was performed in normoxia (21 kPa P_{O_2}) and then a second sample was loaded from the same tonometer for an additional run under hypoxic conditions (3 kPa P_{O_2}). The P_{O_2} value in these hypoxic runs was chosen to yield a Hb-O_2 saturation close to P_{50} and was informed from the previous measurements of Hb-O_2 binding characteristics. Finally, 250 μL of blood were removed from the tonometer for the measurement of blood parameters, as described previously.

Subcellular Localization of RBC β-NHE

To collect RBC samples for immunocytochemistry, the tonometry trial was repeated with RBCs that were suspended in saline instead of plasma and cell fixation was as described previously; this step was necessary as initial trials showed that plasma proteins interfered with the quality of antibody staining (after visual inspection of cell morphology the fixation resulted in satisfactory results for n = 4 out of 6 fish). Fixed RBCs were permeabilized in 1.5 mL 0.1% Triton-X100 (VWR Amresco 1421C243) in PBS for 15 min at room temperature on a revolver rotator. Thereafter, the RBCs were blocked for autofluorescence in 100 mM glycine in PBS for 15 min, after which the cells were rinsed three times in PBS. For immunocytochemistry, 200 μL of these fixed RBCs were resuspended in a blocking buffer containing 3% bovine serum albumin (VWR 0332) and 1% normal goat serum (Lampire Biological Laboratories 7332500; Pipersville) in PBS and incubated for 6 h on a rotator. Primary antibodies were added directly into the blocking buffer and incubated on a rotator overnight at 4°C. A monoclonal mouse anti-Tetrahymena α-tubulin antibody (DSHB12G10; RRID:AB_1157911) was used at 0.24 μg·mL^{-1} and a custom, polyclonal, affinity-purified, rabbit anti-rainbow trout β-NHE antibody (epitope: MERRVSVMERRMSH) was used at 0.02 μg·mL^{-1}. After primary incubations, the RBCs were washed three times in PBS and incubated for 3 h on a rotator at room temperature in blocking buffer containing secondary antibodies: 1:500 goat anti-mouse (AlexaFlour 568; Molecular Probes A-11031, RRID:AB_144696), 1:500 goat anti-rabbit (AlexaFlour 488; Molecular Probes A-11008, RRID:AB_143165) and 1:1,000 4′,6-diamidino-2-phenylindole (DAPI; Roche 10236276001; Basel, Switzerland). After secondary incubations, RBCs were washed three times and were resuspended in PBS. To validate the β-NHE antibody, controls were performed by leaving out the primary antibody and by preabsorbing the primary antibody with its immunizing peptide. All images were acquired with a confocal laser-scanning fluorescence microscope (Zeiss Observer Z1 with LSM 800) and ZEN blue edition software v.2.6. For super-resolution imaging, the cells were resuspended in PBS with a mounting medium (Thermo Fisher Invitrogen ProLong P36980) and acquisition was with the Zeiss AiryScan detector system. To ensure that images were comparable, the acquisition settings were kept identical between the different treatments and between treatments and the controls. Optical sectioning and three-dimensional (3-D) reconstructions of single RBCs from the different treatments were processed with the Imaris software v.9.0. (Imaris, RRID:SCR_007370) and rendered into movies.

Molecular β-NHE Characterization

For Western blotting, RBC crude homogenates were thawed and centrifuged at 16,000 *g* for 1 h at 4°C to obtain a supernatant containing the cytoplasmic fraction and a pellet containing a membrane-enriched fraction that was resuspended in 100 μL of lysis buffer. The protein concentration of all three fractions was measured with the Bradford's assay (Bio-Rad 5000006; Hercules). Samples were mixed 1:1 with Laemmli's sample buffer (Bio-Rad 161-0737) containing 10% 2-mercaptoethanol (Sigma M3148) and were heated to 75°C for 15 min. Sample loading was at 5 μg protein from each fraction for the detection of β-NHE and 60 μg protein from crude homogenate for the detection of α-tubulin, into the lanes of a 5% stacking- and 10% separating polyacrylamide gel (Bio-Rad, MiniProtean Tetra cell). The proteins were separated at 60 V for 30 min and 150 V until the Hb fraction (~16 kDa) ran out of the bottom of the gel (~60 min); previous trials had shown that the high Hb content of these lysates may bind some antibodies nonspecifically. The proteins were transferred onto a Immun-Blot polyvinylidene difluoride membrane (PVDF; Bio-Rad) using a semidry transfer cell (Bio-Rad Trans-Blot SD) overnight, at 90 mA and 4°C. PVDF membranes were blocked overnight, on a shaker at 4°C in Tris-buffered saline with 1% Tween 20 (TBS-T; VWR Amresco ProPure M147) and 0.1 g·mL^{-1} skim milk powder (Kroger; Cincinnati, OH). Primary antibodies were made up in blocking buffer and mixed on a shaker at 4°C, overnight, before applying to the membranes. The anti-α tubulin antibody was used at 4.7 ng·mL^{-1}, the anti-β-NHE antibody at 0.42 ng·mL^{-1}, and controls at a peptide concentration exceeding that of primary antibody by 10:1. Primary incubations were for 4 h on a shaker at room temperature and membranes were rinsed three times in TBS-T for 5 min. Secondary incubations were with either an anti-rabbit or mouse, horseradish peroxidase conjugated secondary antibody (Bio-Rad 1706515, RRID:AB_11125142; and 1706516, RRID:AB_11125547) for 3 h on a shaker at room temperature. Finally, the membranes were rinsed three times in TBS-T for 5 min, and the proteins were visualized by enhanced chemiluminescense (Bio-Rad, Clarity 1705061) in a Bio-Rad Universal III Hood with Image Lab software v.6.0.1 (Image Lab, RRID: SCR_014210). Protein sizes were determined relative to a precision dual-color protein ladder (Bio-Rad 1610374).

The white seabass β-NHE sequence was obtained by transcriptomics analysis of gill samples that were not perfused to remove the blood, and these combined gill and RBC tissue samples were stored in RNA later for processing. Approximately 50 μg of sample were transferred into 1 mL of TRIzol

reagent (Thermo Fisher 15596026) and were homogenized on ice with a handheld motorized mortar and pestle (Kimble Kontes, Düsseldorf, Germany). These crude homogenates were centrifuged at 1,000 *g* for 1 min and the supernatant was collected for further processing. RNA was extracted in RNA spin columns (RNAEasy Mini; Qiagen, Hilden, Germany) and treated with DNAse I (ezDNase; Thermo Fisher, 11766051) to remove traces of genomic DNA. RNA quantity was determined by spectrophotometry (Nanodrop 2000; Thermo Fisher) and RNA integrity was determined with an Agilent 2100 Bioanalyzer (Agilent; Santa Clara, CA). Poly-A enriched complementary DNA (cDNA) libraries were constructed using the TruSeq RNA Sample Preparation Kit (Illumina; San Diego, CA). Briefly, mRNA was selected against total RNA using oligo(dt) magnetic beads and the retained RNA was chemically sheared into short fragments in a fragmentation buffer, followed by first- and second-strand cDNA synthesis using random hexamer primers. Illumina adaptor primers (Forward P5-Adaptor, 5′AATGATACGGCGACCACCGAGA3′; Reverse P7-Adaptor 5′-CGTATGCCGTCTTCTGCTTG-3′) were then ligated to the synthesized fragments and subjected to end-repair processing. After agarose gel electrophoresis, 200–300 bp insert fragments were selected and used as templates for downstream PCR amplification and cDNA library preparation. The combined gill and RBC samples (1 μg RNA) were sent for RNAseq Poly-A sequencing with the Illumina NovoSeq 6000 platform (Novogene; Beijing, China) and raw reads are made available through NCBI (PRJNA722314).

RNAseq data were used to generate a de novo transcriptome assembly, which was mined for white seabass isoforms of the Slc9 protein family using methods described previously (33). Briefly, raw reads were analyzed, trimmed of adaptor sequences, and processed with the OpenGene/fastp software (34), to remove reads: *1*) of low quality (PHRED quality score < 20), *2*) containing >50% unqualified bases (base quality < 5), and *3*) with >10 unknown bases. Any remaining unpaired reads were discarded from downstream analysis and quality control metrics were carried out before and after trimming (raw reads 80.07×10^6; raw bases 12.01 Gb; clean reads 79.44×10^6, clean bases 11.84 Gb, clean reads Q30 95.26%; GC content 46.67%). Thereafter, fastq files were merged into a single dataset, normalized, and used for de novo construction of a combined gill and RBC transcriptome with the Trinity v2.6.6 software (RRID:SCR_013048). Normalization and assembly were performed using the NCGAS (National Centre for Genome Analysis Support) de novo transcriptome assembly pipeline (github.com/NCGAS/de-novo-transcriptome-assembly-pipeline/tree/master/Project_Carbonate_v4) on the Carbonate High Performance Computing cluster at Indiana University. For assembly, minimum kmer coverage was set to three and the minimum number of reads needed to glue two inchworm contigs together, was set to four (35). The resulting nucleotide FASTA file was translated into six protein reading frames using BBMap (RRID:SCR_016965), which were mined for the NHE-like proteins using HMMER3 v.3.0 (hmmer.org) by querying the de novo assembly against a hidden Markov model (HHM) homology matrix generated from 132 aligned protein sequences of the vertebrate NHE family (Slc9a1–Slc9a9; for accession numbers see Supplemental Table S1; all Supplemental Tables, Figures, and Movies are available at https://doi.org/10.6084/m9.figshare.15505941.v1). Sequences were aligned using MUSCLE (RRID:SCR_011812) in SeaView (RRID:SCR_015059), with NHE2 from *Caenorhabditis elegans* as an outgroup, and results were refined using GBlocks (36) according to the parameters specified previously (37). Phylogenetic analysis was conducted on the Cyberinfrastructure for Phylogenetic Research (CIPRES) Science Gateway (38) using the RAxML software v.8.2.12 (RRID:SCR_006086) with the LG evolutionary and GTRGAMMA models (39). Branch support was estimated by bootstraps with 450 replications and the constructed tree was edited in FigTree v.1.4.4 (RRID:SCR_008515). Finally, the open reading frame of the white seabass β-NHE sequence (predicted 747 amino acids) was analyzed for the presence of the Kozak nucleic acid motifs [5′-(gcc)gccRccAUGG-3′] (40) immediately upstream of putative start codons, using the ATGpr software (41).

To confirm the expression of the β-NHE in the RBCs of white seabass, an additional blood sample of 1 mL was collected and processed as described previously. RBCs were lysed by repeatedly passing them through a 23-gauge needle and RNA extraction was on 50 μg of RBCs by standard TRIzol and chloroform extraction following the kit instructions. Isolated RNA was treated with DNAse I, and 1 μg RNA was used to synthesize first-strand cDNA using SuperScript IV reverse transcriptase (Thermo Fisher 18090010). Full-length cDNA sequences were obtained in 35 cycles of PCR reactions with Phusion DNA polymerase (New England Biolabs, Ipswich; MO531L) and specific primers designed against the sequence of the phylogenetically characterized white seabass β-NHE obtained from the combined gill and RBC transcriptome (Integrated DNA Technologies, Coralville, IA; F: 5′-TCC CGT ACT ATC CTC ATC TTC A-3′ R: 5′-CCT CTG CTC TCT GAA CTG TAA AT-3′). Amplicons were analyzed by gel electrophoresis (Bio-Rad ChemiDoc) that confirmed the presence of a single band (2,372 bp; Supplemental Fig. S1). A-overhangs were added to Phusion products with one unit Taq polymerase (New England Biolabs; MO267S) followed by 10 min incubation at 72°C. Products were cloned (TOPO TA Cloning Kit/pCR 2.1-TOPO Vector; Invitrogen; K4500) and the ligated product was transformed into TOP10 chemically competent *Escherichia coli* cells (Invitrogen; K457501) according to the manufacturer's specifications. After an overnight incubation at 37°C, single colonies of transformants were grown in Luria-Bertani (LB) broth overnight on a shaking incubator (37°C, 220 rpm; Barnstead MaxQ 4000). Plasmid DNA was isolated (PureLink Quick Plasmid Miniprep kit; Invitrogen K210010) according to the manufacturer's specifications and inserts were sequenced to confirm their identity and uploaded to NCBI (MW962257).

Calculations and Statistical Analysis

All data were analyzed with R v.4.0.4 (RRID:SCR_001905) in RStudio v.1.4.1106 (RRID:SCR_000432), and figures were created with the ggplot2 package (RRID:SCR_014601). Normality of the residuals was tested with the Shapiro–Wilk test (stat.desc function in R) and homogeneity of variances was confirmed with the Levene's test (leveneTest function in R). Deviations from these parametric assumptions were

corrected by transforming the raw data as described next. All raw data and R source code are made publicly available (see https://doi.org/10.6084/m9.figshare.15505965.v1).

To determine the blood O_2-binding characteristics, Hb P_{50} and Hill coefficient (n_H) values were those determined with the BOBS software v.1.0.20 (Loligo) and oxygen equilibrium curves (OEC) were generated by fitting a two parameter Hill function to the mean P_{50} and n_H for eight individual fish. The main effects of P_{CO_2} on P_{50} and n_H were analyzed by analysis of covariance (ANCOVA, $P < 0.05$, $n = 8$). Plasma [HCO_3^-] was calculated from TCO_2 by subtracting the molar [CO_2] calculated from the dissociation constant and solubility coefficients in plasma at 17°C and the corresponding sample pH (6). The Bohr effects relative to pH_i and pH_e, the relationship between RBC pH_i and pH_e, and the nonbicarbonate buffer capacity of whole blood were determined by linear regression analysis, results of which are shown in detail in the Supplemental Fig. S2, *A*–*D*. The average values for these blood parameters are shown in the main text and were calculated as the average slopes across all individuals.

In the RBC swelling trial, mean cell Hb content (MCHC) was calculated as [Hb] divided by Hct as a decimal. Since Hb is a membrane impermeable solute, MCHC is used as a common indicator of RBC swelling. Main effects of drugs (DMSO, ISO, and ISO + Am), time (10, 30, and 60 min), and their interaction (drug × time) on Hct, [Hb], MCHC, pH_e, and pH_i were determined by two-way ANOVAs (lm and Anova functions in *R*; $n = 5$ or 6; $P < 0.05$) and multiple comparisons were conducted with *t* tests (pairwise.*t*.test function in *R*) and controlling the false detection likelihood (FDR) with a Benjamini–Hochberg correction (*P*.adjust function in *R*).

The effect of RBC β-adrenergic stimulation on Hb-O_2 binding was assessed by analyzing the absorbance data from the BOBS in *R* (R source code available at https://doi.org/10.6084/m9.figshare.15505965.v1). In brief, the absorbances recorded at 430 nm were divided by the isosbestic wavelength of 390 nm (where absorbance is independent of Hb-O_2 binding), and these ratios were used as the raw data for subsequent analyses. For each trace, the ten final absorbance ratios at each equilibration step were averaged (i.e., 10 s) and Hb-O_2 saturation was calculated relative to the absorbance at the two initial calibration conditions (i.e., high: 99.7 kPa P_{O_2}, 0.3 kPa P_{CO_2}; and low: 0 kPa P_{O_2}, 0.3 kPa P_{CO_2}), assuming full saturation or desaturation of Hb, respectively. These calibration values were measured again at the end of each trial and a linear correction of drift was performed for each sample. The resulting values for Hb-O_2 saturation were plotted against P_{CO_2} and several nonlinear models were fit to the data (Michaelis–Menten, Exponential, and Hill). The model with the best fit (lowest Akaike information criterion; AIC) was a three-parameter Hill function that was applied to each individual trace. The parameter estimates from this model yielded the maximal reduction in Hb-O_2 saturation (Max. ΔHb-O_2 sat.; %) in normoxia (21 kPa P_{O_2}) and hypoxia (3 kPa P_{O_2}), and the P_{CO_2} at which this response was half-maximal (EC_{50} P_{CO_2}; kPa); for the latter, raw data was log-transformed to meet the parametric assumptions during statistical analysis. The main effects of drugs (DMSO, ISO, and ISO + Am), O_2 (normoxia and hypoxia), and their interaction (drug × O_2), on the parameter estimates from the Hill functions were determined by two-way ANOVAs (lm and Anova functions in *R*; $n = 6$; $P < 0.05$). When significant main effects were detected, multiple comparisons were conducted with *t* tests and controlling the false detection likelihood (FDR) with a Benjamini–Hochberg correction. The Root effect was expressed as the degree of Hb-O_2 desaturation (%) during hypercapnic acidification of blood in normoxia, and was determined from the nonlinear model, as the Max. ΔHb-O_2 sat. of the control treatment (DMSO), which represents the asymptotic value at which further acidification does not affect Hb-O_2 sat. (42). To quantify the relative changes in Hb-O_2 saturation (ΔHb-O_2 sat.) due to drug treatments, data were expressed relative to the paired measurements in the DMSO treatment for each individual fish and relative to the initial Hb-O_2 saturation at arterial P_{CO_2} (0.3 kPa). All data are presented as means ± SE.

RESULTS

Blood O_2-Binding Characteristics

The blood O_2-binding characteristics of white seabass are summarized in Fig. 1. When P_{CO_2} was increased from arterial tension (0.3 kPa) to severe hypercapnia (2.5 kPa) Hb P_{50} increased significantly from 2.9 ± 0.1 to 11.8 ± 0.3 kPa. At the same time, the cooperativity of Hb-O_2 binding, expressed by n_H, decreased significantly from 1.52 ± 0.04 to 0.84 ± 0.03, which was reflected in a change in the shape of the OECs from sigmoidal to hyperbolic. Over the tested range of P_{CO_2}, white seabass displayed a Bohr coefficient of −0.92 ± 0.13 when expressed relative to the change in pH_e (which is a common way to report these values) and −1.13 ± 0.11 when expressed relative to the change in RBC pH_i (which is the in vivo relevant value; Supplemental Fig. S2, *A* and *B*). In

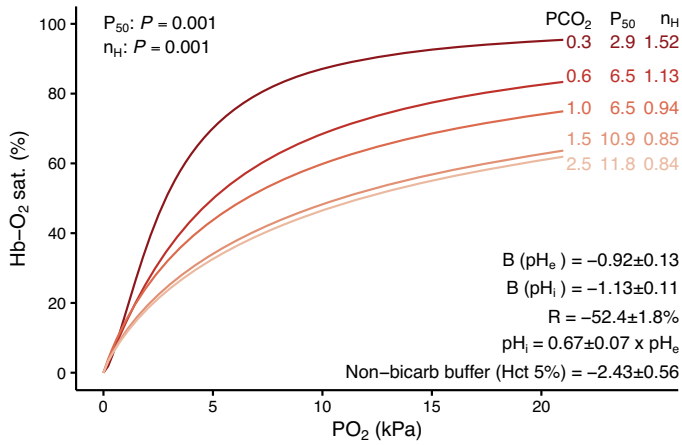

Figure 1. Oxygen-binding characteristics of white seabass whole blood. Oxygen equilibrium curves showing hemoglobin-oxygen saturation (Hb-O_2 sat.; %) as a function of the partial pressure of oxygen (P_{O_2}; kPa) at five partial pressures of carbon dioxide (P_{CO_2}). The P_{O_2} that yields 50% Hb-O_2 saturation (P_{50}) and the cooperativity coefficient of Hb-O_2 binding (Hill coefficient, n_H) are shown for each curve. The main effects of P_{CO_2} on P_{50} and n_H were analyzed with ANCOVA ($P < 0.05$, $n = 8$ fish). The Bohr coefficients (B) relative to extracellular (pH_e) and intracellular (pH_i), the relationship between pH_e and pH_i, and the nonbicarbonate buffer capacity of the blood (at 5% Hct) were determined by linear regressions (see Supplemental Fig. S2). The Root effect (*R*) was determined at 21 kPa P_{O_2} from the model parameters shown for the DMSO treatment in Fig. 6*B*. All data are means ± SE.

addition, white seabass blood showed a large reduction in Hb-O_2 saturation during normoxic acidification at high P_{CO_2}. The magnitude of this Root effect was predicted by a nonlinear model, with a maximal reduction in Hb-O_2 saturation of 52.4 ± 1.8%. The relationship between pH_i and pH_e had a slope of 0.67 ± 0.07 (Supplemental Fig. S2*C*), reflecting the higher buffer capacity of the intracellular space. The nonbicarbonate buffer capacity of white seabass whole blood was −2.43 ± 0.56 mmol·L^{-1}·pH_e^{-1} at a Hct of 5% (Supplemental Fig. S2*D*). By correcting this value for the higher Hct in vivo, according to Wood et al. (43), white seabass with a Hct of 25% are expected to have a whole blood nonbicarbonate buffer capacity of −9.68 mmol·L^{-1}·pH_e^{-1}.

RBC Swelling after β-Adrenergic Stimulation

The β-adrenergic stimulation of white seabass blood with ISO induced changes in the measured blood parameters (Fig. 2). Significant main effects of drug, time, and their interaction (drug × time) indicate that Hct was affected by the experimental treatments (Fig. 2*A*). A large increase in Hct was observed in ISO-treated blood that was absent in ISO + Am and DMSO-treated RBCs. In addition, a main effect of drug treatments on MCHC indicated that the increase in Hct after ISO addition was due to swelling of the RBCs (Fig. 2*B*), whereas [Hb] was not affected by the treatments (Supplemental Fig. S3). Significant main effects of drug and time were also detected for pH_e, where a large extracellular acidification was observed in ISO-treated blood, relative to the DMSO and ISO + Am treatments (Fig. 2*C*). No significant main effect of drug or time were observed on RBC pH_i, but multiple comparisons indicated a trend for a higher pH_i in ISO compared with DMSO-treated blood (P = 0.081; Fig. 2*D*). Differential interference contrast (DIC) images confirmed a normal morphology of the RBCs at the beginning and the end of the trials, thus validating the fixation procedure. Swelling was observed in ISO-treated RBCs, relative to initial measurements, or DMSO and ISO + Am-treated cells (Fig. 2, *E–H*). The swelling of ISO-treated RBCs occurred largely

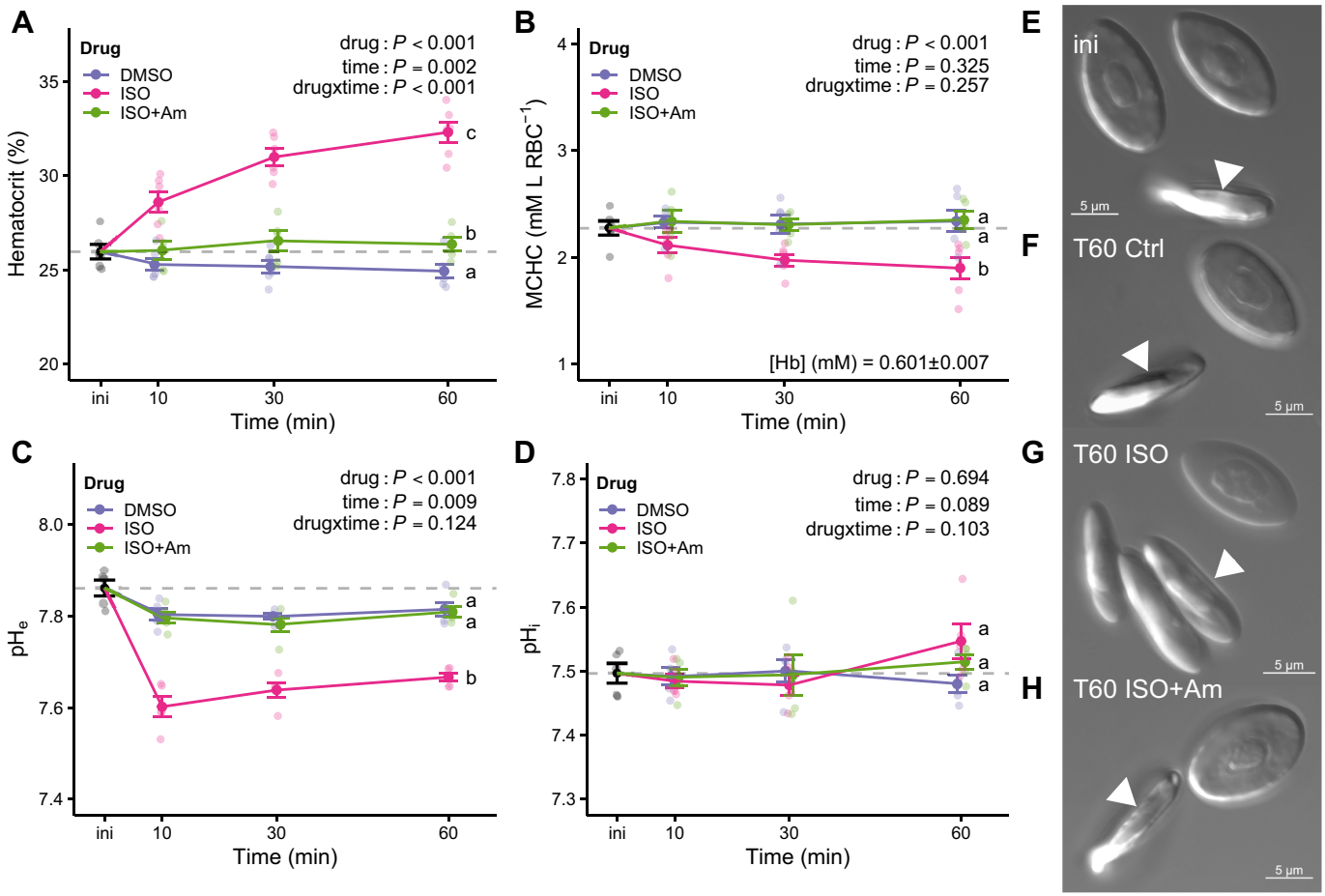

Figure 2. Changes in blood parameters after adrenergic stimulation of white seabass whole blood. Hematocrit (%) (*A*), mean cell hemoglobin content (MCHC; mM hemoglobin·L^{-1} red blood cells^{-1}) (*B*), extracellular pH (pH_e) (*C*), and intracellular pH (pH_i) (*D*). Blood was equilibrated in tonometers at 3 kPa P_{O_2} and 1 kPa P_{CO_2} and treated with either of the following: *1*) a carrier control (dimethyl sulfoxide, DMSO; 0.25%), *2*) the β-adrenergic agonist isoproterenol (ISO; 10 µM), or *3*) ISO plus amiloride (ISO + Am; 1 mM), an inhibitor of sodium-proton exchangers (NHEs). The dotted line indicates initial values for each parameter and changes were recorded over 60 min. The main effects of drug, time, and their interaction term (drug × time) were analyzed with a two-way ANOVA ($P < 0.05$, n = 6 fish and n = 5 for ISO + Am). There were no significant changes in hemoglobin concentration ([Hb]; mM) throughout the trials. Multiple comparisons were with paired t tests with a Benjamini–Hochberg correction and superscript letters that differ indicate significant differences between treatments at 60 min. Individual datapoints and means ± SE. *Insets E–H*: differential interference contrast (DIC, ×60) images of red blood cells fixed at the beginning (ini) and the end of the trial (T60). Cell swelling was visually confirmed in ISO-treated cells, but not in other treatments, and mostly along the *z*-axis of the cells (arrows), while the *x-y* axis seemed largely unaffected.

along the *z*-axis of the cells (indicated by the arrows), whereas no visible distortion was observed in the *x*-*y* directions.

Molecular β-NHE Characterization

The combined gill and RBC de novo transcriptome of white seabass contained nine Slc9 transcripts and phylogenetic analysis placed these sequences within well-supported clades of the NHE family tree (Fig. 3). Importantly, one of these white seabass transcripts grouped with the Slc9a1b sequences from other teleost fishes, supporting its classification as a white seabass β-NHE. Results from RT-PCR, cloning, and sequencing confirmed the expression of β-NHE mRNA in isolated white seabass RBCs. A search for the Kozak nucleic acid motif in the open reading frame of the white seabass β-NHE sequence yielded the five most likely potential start codons, including one that would produce a 66-kDa protein (Supplemental Table S2). This size closely matched the single band that was specifically recognized by the polyclonal β-NHE antibody in Western blots with crude

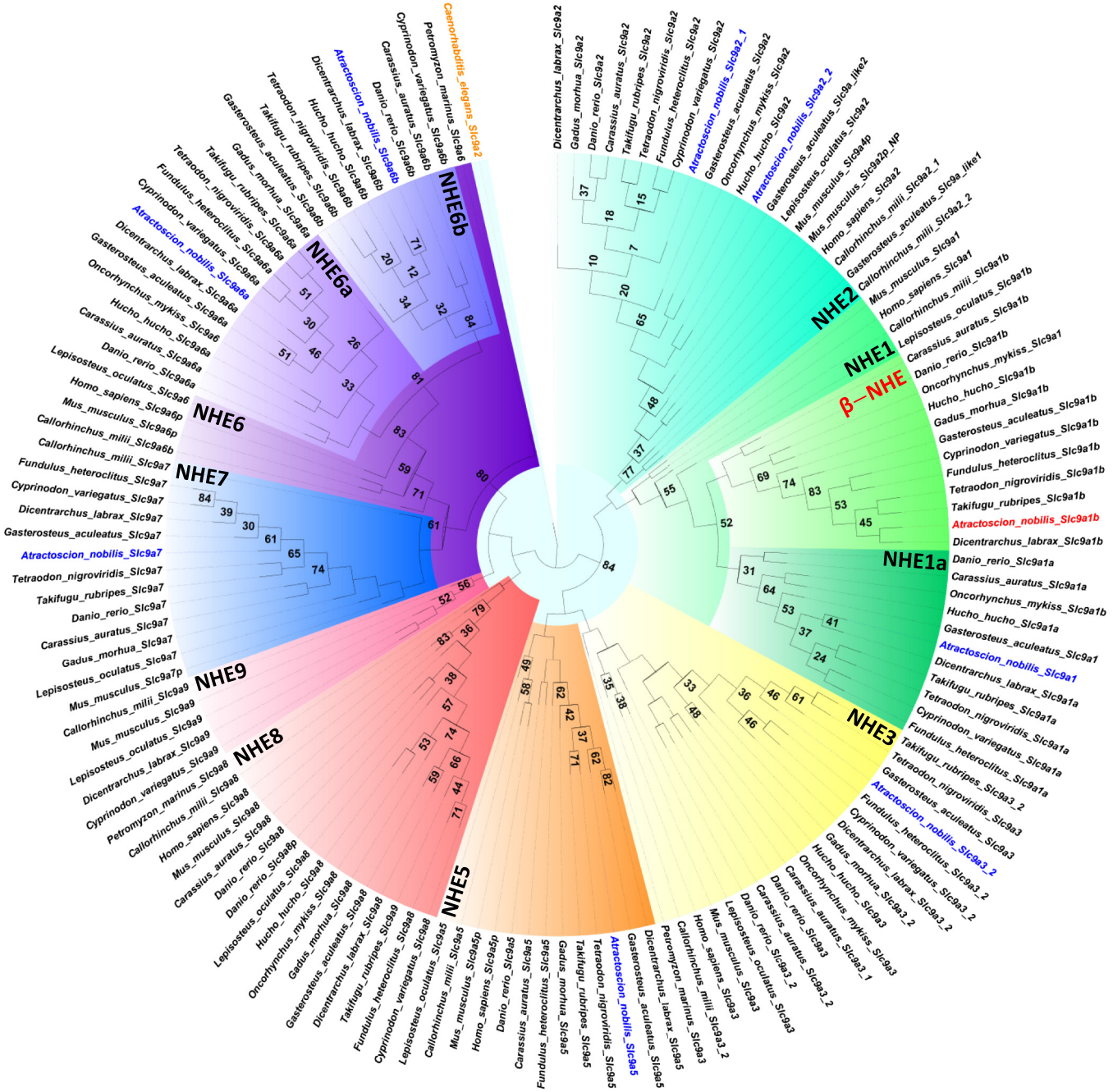

Figure 3. Phylogenetic analysis of nine sodium-proton exchanger (NHE)-like protein sequences in the de novo assembly of a combined white seabass gill and red blood cell transcriptome. Novel white seabass sequences are highlighted in blue and the β-NHE in red (Slc9a1b). Background shadings delineate subfamilies of the Slc9 gene family and bootstrap values are indicated at the nodes. The tree was rooted against the NHE2 from *Caenorhabditis elegans* in orange. Accession numbers for all species are those reported in Supplemental Table S1.

homogenate, cytosolic, and membrane-enriched fractions of a white seabass RBC lysate (Supplemental Fig. S4*A*); whereas no immunoreactivity was observed in lanes where the antibody had been preabsorbed with its immunizing peptide. The anti-α-tubulin antibody detected a single band in the RBC crude homogenate, at the predicted size of 54 kDa (Supplemental Fig. S4*B*). Finally, the white seabass β-NHE protein sequence shared seven consecutive amino acids with the peptide used to raise the polyclonal antibodies (Supplemental Fig. S4*C*), which is sufficient for specific antibody binding (44). More importantly, the antigen peptide sequence was absent in the other eight white seabass NHE isoforms, ruling out nonspecific antibody recognition of these NHEs.

Subcellular Localization of RBC β-NHE

The subcellular location of β-NHE protein in white seabass RBCs was determined by immunofluorescence cytochemistry and super-resolution confocal microscopy (Fig. 4). In DMSO-treated RBCs, the β-NHE immunolabeling was most intense in intracellular vesicle-like structures, and fainter at the plasma membrane. There was substantial heterogeneity in the staining pattern for β-NHE in these control cells, with varying amounts of intracellular and membrane staining. In ISO-treated RBCs, the staining pattern for β-NHE was more homogeneous and most cells showed strong immunoreactivity for β-NHE in the membrane that colocalized with α-tubulin in the marginal band, and the intracellular, vesicle-like staining that was observed in the control cells was reduced (see Supplemental Fig. S5 for an overview image with more cells). In contrast, ISO-treated cells that were incubated without the primary antibody or where the antibody was preabsorbed with its immunizing peptide showed no immunoreactivity for β-NHE (Supplemental Fig. S6). Finally, optical sectioning and three-dimensional reconstruction of these RBCs confirmed that the membrane staining for β-NHE occurred in a single plane and colocalized with α-tubulin in the marginal band (see Supplemental Movies S1 and S2).

Hb-O_2 Binding after β-Adrenergic Stimulation

To characterize the protective effect of RBC β-NHE activation on Hb-O_2 binding, blood samples were first equilibrated to 21 kPa P_{O_2} and 0.3 kPa P_{CO_2} in tonometers and no significant effects of drug treatment (DMSO, ISO, or ISO + Am) were observed on any of the initial blood parameters (Supplemental Fig. S7); average values were the following: Hct 5.20 ± 0.14% (P = 0.095), [Hb] 0.178 ± 0.006 mM (P = 0.889), MCHC 3.46 ± 0.15 mM·L^{-1} RBC (P = 0.490), pH_e 7.848 ± 0.018 (P = 0.576), pH_i 7.464 ± 0.021 (P = 0.241). Thereafter, blood was loaded into the BOBS, where Hb-O_2 saturation was measured spectrophotometrically at increasing levels of a respiratory acidosis in normoxia (21 kPa P_{O_2}). As expected from the pH sensitivity of Hb-O_2 binding in white seabass, an increase in P_{CO_2} from 0.3 to 3 kPa caused a severe reduction in Hb-O_2 saturation in all treatments, via the Root effect (Fig. 5). Results were analyzed by fitting a three-parameter Hill model to the individual observations within each treatment and significant differences were observed in the parameter estimates that describe these data. EC_{50} P_{CO_2} was affected by the experimental treatments, as shown in a significant main effect of drug (Fig. 6*A*). Multiple comparisons confirmed significant differences in EC_{50} P_{CO_2} which was 0.85 ± 0.06 kPa in DMSO, 0.91 ± 0.06 kPa in ISO + Am, and 1.08 ± 0.06 kPa in ISO-stimulated blood. In contrast, the

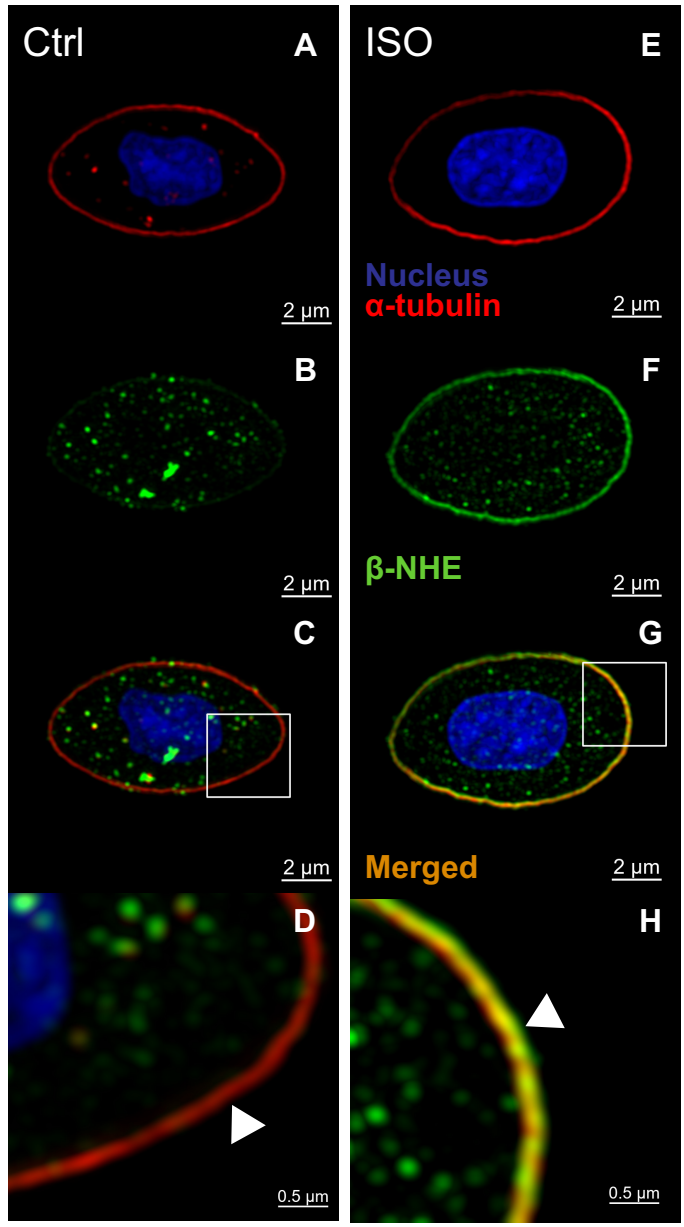

Figure 4. Immunocytochemical localization of the β-adrenergic sodium-proton exchanger (β-NHE) in white seabass red blood cells. Blood was equilibrated in tonometers at 3 kPa P_{O_2} and 1 kPa P_{CO_2} for 60 min (see Fig. 2 for details) in the presence of either of the following: a carrier control (dimethyl sulfoxide, DMSO; 0.25%) (*A*–*D*), or the β-adrenergic agonist isoproterenol (ISO; 10 μM) (*E*–*H*). Fixed cells were immunostained with a monoclonal α-tubulin antibody to visualize the marginal band (red), with DAPI to visualize the cell nuclei (*A* and *E*), and with a polyclonal anti-β-NHE antibody (green, *B* and *F*). *D* and *H*: magnified view of the *insets* in the merged images, where arrows indicate weak or absent β-NHE immunoreactivity on the membrane of Ctrl cells and intense staining in ISO-treated cells. These responses were representative and repeatable (n = 4 fish) and images showing a larger number of cells are available in Supplemental Fig. S5.

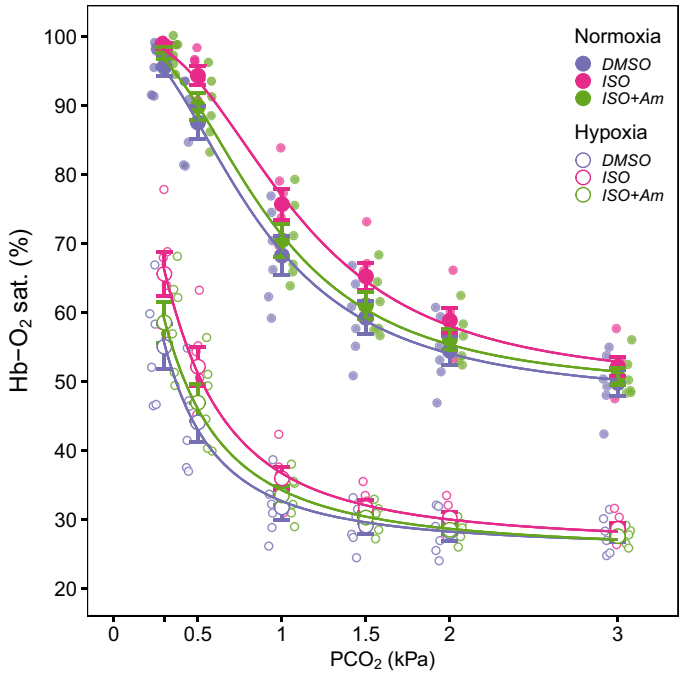

Figure 5. Hemoglobin-oxygen saturation (Hb-O_2 sat.; %) during hypercapnic acidification of white seabass whole blood. Hematocrit was set to 5%, blood was equilibrated in tonometers at 21 kPa P_{O_2} and 0.3 kPa P_{CO_2} and treated with either of the following: *1*) a carrier control (dimethyl sulfoxide, DMSO; 0.25%), *2*) the β-adrenergic agonist isoproterenol (ISO; 10 μM), or *3*) ISO plus amiloride (ISO + Am; 1 mM), an inhibitor of sodium-proton exchangers (NHE). For each sample, runs were performed in normoxia (21 kPa P_{O_2}) or hypoxia (3 kPa P_{O_2}). Individual datapoints and means ± SE. (n = 6 fish).

magnitude of the responses, Max. ΔHb-O_2 sat., was not affected by the experimental treatments and no significant main effect of drug was detected; the average Max. ΔHb-O_2 sat. across treatments was −51.1 ± 0.7% (Fig. 6*B*).

When the same experiment was repeated under hypoxic conditions (3 kPa P_{O_2}), an increase in P_{CO_2} likewise caused a severe reduction in Hb-O_2 saturation, indicating that in white seabass, a Root effect can also be expressed at saturations around P_{50} (Fig. 5). A significant main effect of O_2 indicated that cells in the hypoxic condition required a lower EC_{50} P_{CO_2} to achieve Max. ΔHb-O_2 sat. compared with the normoxic condition (Fig. 6*A*). There was also a significant main effect of drug on EC_{50} P_{CO_2} and multiple comparisons indicated a similar pattern in the individual drug effects as in the normoxic experiment, which was further confirmed by the absence of a significant drug × O_2 interaction. Finally, a significant effect of O_2 on Max. ΔHb-O_2 sat. (Fig. 6*B*) indicated a larger response magnitude in hypoxic blood, but that was unaffected by drug treatments, and the average Max. ΔHb-O_2 sat. across treatments was −74.1 ± 0.1%.

To quantify the protective effect of RBC β-NHE activation on Hb-O_2 binding during a hypercapnic acidosis, Hb-O_2 saturation was expressed relative to the paired measurements in the DMSO treatment for each individual fish and relative to the initial Hb-O_2 saturation at 0.3 kPa P_{CO_2} (i.e., 95.6% and 55.0% Hb-O_2 saturation in normoxia and hypoxia, respectively; Fig. 5). In normoxia, the benefit of β-NHE stimulation with ISO showed a bell-shaped relationship with a maximal ΔHb-O_2 sat. of 7.8 ± 0.02% at 1 kPa P_{CO_2} (Fig. 7*A*). When NHEs were inhibited in ISO + Am-treated blood, ΔHb-O_2 sat. was only 1.9 ± 0.4% at 1 kPa P_{CO_2} and significantly lower compared with the other treatments; at higher P_{CO_2} the 95% confidence intervals overlapped with the DMSO values, indicating no difference from controls. In hypoxic blood, the ISO treatment had the largest effects on ΔHb-O_2 sat. at 0.3 kPa P_{CO_2}, with maximal values of 19.2 ± 0.0% that decreased toward higher P_{CO_2} (Fig. 7*B*). Whereas, in the ISO + Am treatment, ΔHb-O_2 sat. was 6.4 ± 0.0% at 0.3 kPa P_{CO_2}, and significant differences to the DMSO controls were only observed at P_{CO_2} below 1.5 kPa.

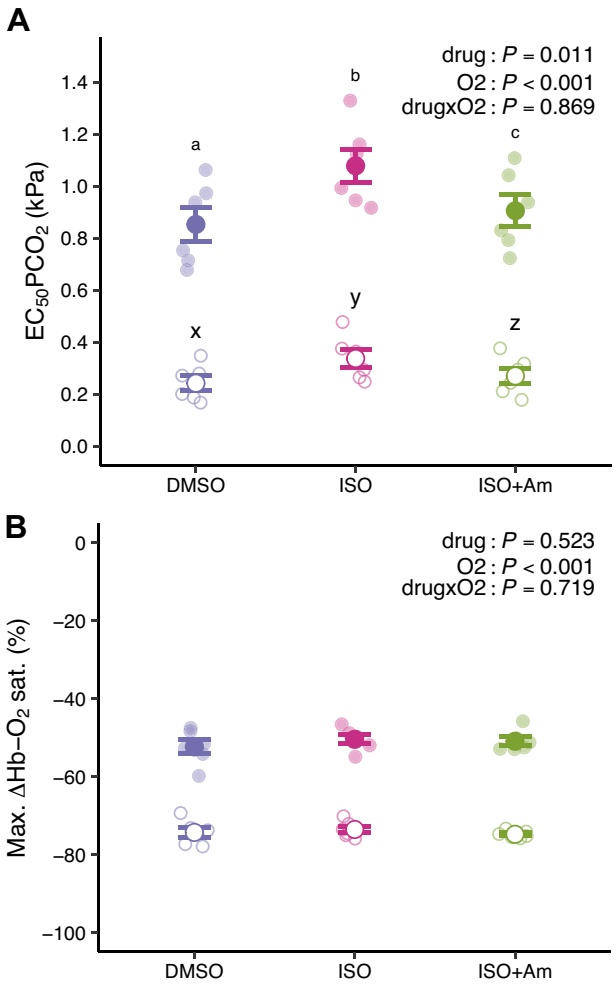

Figure 6. Parameter estimates describing the changes in hemoglobin-oxygen (Hb-O_2) saturation during hypercapnic acidification of white seabass whole blood. The P_{CO_2} that elicits a half-maximal reduction in Hb-O_2 saturation (EC_{50} P_{CO_2}; kPa) (*A*) and the maximal reduction in Hb-O_2 saturation due to acidification (Max. ΔHb-O_2 sat.; %) (*B*). Treatments were the following: *1*) a carrier control (dimethyl sulfoxide, DMSO; 0.25%), *2*) the β-adrenergic agonist isoproterenol (ISO; 10 μM), or *3*) ISO plus amiloride (ISO + Am; 1 mM) an inhibitor of sodium-proton exchangers (NHE). For each sample, runs were performed in normoxia (21 kPa P_{O_2}; solid symbols) or hypoxia (3 kPa P_{O_2}; open symbols). The main effects of drug treatments (drug), oxygen (O_2) and their interaction term (drug × O_2) were analyzed with a two-way ANOVA ($P < 0.05$, n = 6 fish). Multiple comparisons were with paired t tests and a Benjamini–Hochberg correction and superscript letters that differ indicate significant differences between treatments for each O_2 tension. Individual data points and means ± SE.

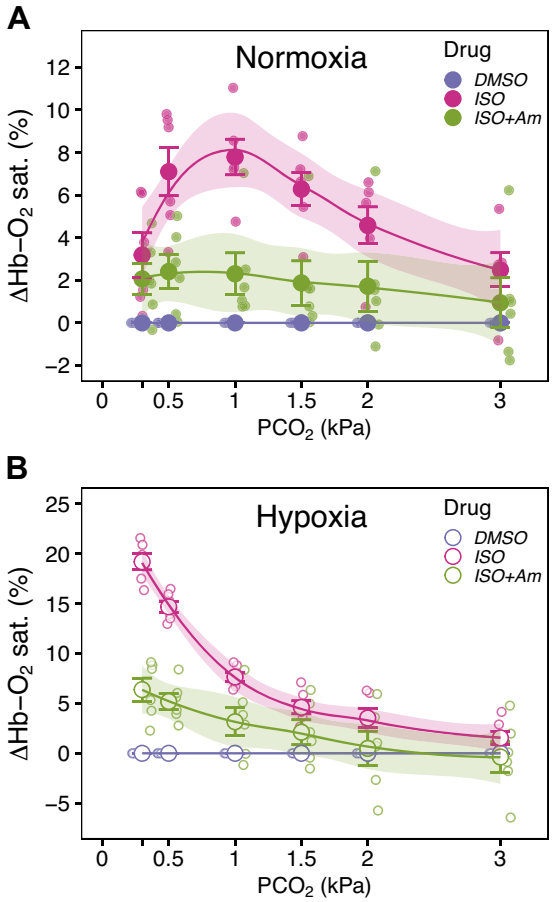

Figure 7. Relative changes in hemoglobin-oxygen saturation (ΔHb-O_2 sat.; %) during hypercapnic acidification of white seabass whole blood. In normoxia (21 kPa P_{O_2}) (*A*) or hypoxia (3 kPa P_{O_2}) (*B*). Treatments were the following: *1*) a carrier control (dimethyl sulfoxide, DMSO; 0.25%), *2*) the β-adrenergic agonist isoproterenol (ISO; 10 μM), or *3*) ISO plus amiloride (ISO + Am; 1 mM), an inhibitor of sodium-proton exchangers (NHE). Individual data points, means ± SE and 95% confidence intervals (n = 6 fish).

DISCUSSION

A novel finding from the present study was the subcellular localization of β-NHE protein in intracellular, vesicle-like structures within the RBCs of white seabass. Upon adrenergic stimulation this pool of β-NHE protein was translocated and incorporated into the RBC membrane, which represents a novel cellular pathway for the regulation of β-NHE activity that may not require posttranslational modifications of the protein itself. These findings, and the presence of a RBC β-NHE in white seabass were further corroborated by molecular and phylogenetic data, and functional measurements of β-NHE activity were performed in a physiologically and ecologically relevant context. In line with our initial hypothesis, RBC β-NHE activity in white seabass may greatly protect the blood O_2-carrying capacity during environmental hypoxia and hypercapnia. However, not all predictions were met as expected: white seabass did not have an unusually high Hb-O_2 affinity and thus, other aspects of their physiology are likely more important in determining their tolerance to hypoxia. Like other teleosts, white seabass had highly pH-sensitive Hbs, where a reduction in pH decreased both Hb-O_2 affinity via the Bohr effect and Hb-O_2 carrying capacity via the Root effect. A detailed quantification of the protective effects of RBC β-NHE activity revealed that the largest benefits in normoxia (21 kPa P_{O_2}) occurred at ~1 kPa P_{CO_2}, where Hb-O_2 saturation increased by ~8%. The effects were even greater in hypoxia (3 kPa P_{O_2}), where β-NHE activity increased Hb-O_2 saturation by ~20%, but only at arterial P_{CO_2} (0.3 kPa). In hypoxia, the benefits of β-NHE activation decreased rapidly with progressive hypercapnia, revealing an ecologically relevant vulnerability of white seabass to combinations of these stressors.

Subcellular Translocation of β-NHE Protein

Several lines of evidence in our study indicate the presence of functional β-NHEs in white seabass RBCs. Fixed RBCs were studied in detail by super-resolution microscopy and by immunolabeling β-NHE and α-tubulin (Fig. 4), and all RBCs showed β-NHE immunoreactivity, confirming the presence of β-NHE protein in these cells. In control RBCs, β-NHE protein was detected intracellularly and appeared to be confined to vesicles-like compartments, while fainter staining was detected on the plasma membrane of some cells (Fig. 4*B* and Supplemental Fig. S5). A similar staining pattern has been described for a NHE1-like protein in the RBCs of winter flounder (*Pseudopleuronectes americanus*) (45). However, the immunolabeling of NHEs was with polyclonal antibodies raised against a region of the human NHE1 sequence (aa 631–746) that is highly conserved within other members of the teleost NHE protein family (including Slc9a1a and Slc9a1b). Therefore, these previous results likely show staining of several NHE isoforms including the flounder β-NHE. In contrast, the antibody used in the present study had a high specificity for the white seabass β-NHE (Supplemental Fig. S4) and a confounding detection of other RBC NHE isoforms is unlikely.

An important finding of our work was that the intracellular localization of β-NHE protein changed after adrenergic stimulation of the RBCs. In ISO-treated cells the staining pattern for β-NHE was more homogeneous compared with controls, with strong signal at the plasma membrane, and weaker intracellular signal (Fig. 4*F* and Supplemental Fig. S5). Optical sectioning and 3-D reconstructions of these cells clearly showed that the intense membrane staining for β-NHE was confined to a single plane, colocalizing with α-tubulin in the marginal band, and that this signal was mostly absent in DMSO-treated cells (Supplemental Movies S1 and S2). Furthermore, the use of super-resolution microscopy allowed us to discern the subcellular orientation of the β-NHE signal, which was extracellular relative to α-tubulin (Fig. 4*H*), thus, indicating a direct contact with the blood plasma that is essential for regulating pH_i via NHE activity. Combined, these observations point toward an adrenergically induced translocation of β-NHE protein from the cytoplasm into the membrane of white seabass RBCs. Intracellular translocation of NHEs in response to various stimuli has been reported in other systems, such as the gills of acid-infused hagfish (45), insulin-treated rat cardiomyocytes (46), isolated mammalian cells after acidification (47), or the initiation of Na^+-glucose cotransport in intestinal epithelial cells (48). In addition, previous work on teleosts found

that the abundance of radiolabeled β-NHE protein in the membrane of rainbow trout RBCs increased after hypoxic incubation (1.2 kPa for 30 min) (49), which is consistent with protein translocation. However, our work found no evidence for translocation due to a hypoxia stimulus and instead, we show for the first time, that RBC β-NHE in a teleost are translocated after adrenergic stimulation. In the previous report of RBC NHE staining in flounder (50), blood was obtained by caudal puncture, which has been shown to trigger the release of catecholamines and the stimulation of β-NHEs (26). Based on our finding this may have induced changes in the intracellular localization of NHEs, yielding an intense membrane staining, which resembles our results after adrenergic stimulation. The colocalization of β-NHE and α-tubulin protein in the marginal band of RBCs may indicate an involvement of the cytoskeleton in the translocation of vesicles, which may constitute a more general mechanism to modulate membrane protein activity in vertebrate RBCs and importantly, one that does not require conformational changes of the transporters themselves. Clearly, there are still many open questions regarding the well-studied β-NHE response of teleosts, and additional work is required to characterize the cellular mechanisms underlying the translocation of β-NHE protein and its regulation by catecholamines, P_{O_2}, P_{CO_2}, or pH. If substantiated, our findings may open new avenues in the research of RBC physiology in teleosts and perhaps other vertebrates.

To corroborate our microscopy results and the presence of a β-NHE in white seabass, we generated a combined gill and RBC transcriptome that detected nine sequences belonging to the vertebrate NHE (Slc9) family, and phylogenetic analysis classified the white seabass Slc9a1b transcript as belonging to the larger group of teleost RBC β-NHEs (Fig. 3). These findings were further supported by the results from RT-PCR, confirming the expression of a β-NHE in white seabass RBCs. Western blots with a polyclonal anti-trout β-NHE antibody recognized a single band at 66 kDa in white seabass RBC homogenates (Supplemental Fig. S4*A*), which is smaller than the 84 kDa predicted based on the longest possible mRNA transcript (Supplemental Table S2). However, a search for Kozak motifs revealed the five most likely potential start codons in the open reading frame of the white seabass β-NHE mRNA sequence, one of which predicted a protein size of 66 kDa that matches the protein size detected in Western blots. This predicted β-NHE isoform lacks 158 amino acids on the NH_2-terminus, which, according to structural NHE-protein models (51) are not essential for the transporter's activity, but may determine a differential sensitivity to inhibitors (51, 52). NHE isoforms from other teleosts have also been shown to separate in Western blotting with a similar size discrepancy (53) and show differential sensitivity to amiloride and its derivatives compared with mammalian NHEs (54).

Characterization of Hb-O_2 Binding in White Seabass

Many hypoxia tolerant vertebrates have evolved Hbs with a high affinity for O_2 (low Hb P_{50} values), which helps them extract the gas from the respiratory medium (9, 55, 56). White seabass in the present study had a Hb P_{50} of 2.9 ± 0.1 kPa (Fig. 1), which is higher than the values typically found in hypoxia tolerant fishes, such as carp (*Cyprinus carpio*) that have Hb P_{50} values as low as 0.5 kPa (57). In fact, the Hb P_{50} of white seabass resemble more closely the values in the well-studied rainbow trout, of 3.3 kPa (58), a cold-stream salmonid, of no noteworthy hypoxia tolerance. However, marine teleosts tend to have higher Hb P_{50} compared with fresh water species and the adaptive significance of differences in Hb-O_2 affinity must be interpreted with some caution (59). The O_2-binding affinity of Hb must strike a balance between loading O_2 at the gas exchange surface and unloading O_2 at the tissues (60). Everything else being equal, a higher Hb P_{50} can sustain a higher P_{O_2} at the tissue capillaries, enhancing the diffusion gradient of O_2 to the mitochondria, which is of particular benefit to those species with a high scope for exercise (61). Thus, it seems that a high Hb-O_2 affinity is not part of the physiological mechanisms that facilitates hypoxia tolerance in white seabass, but instead, a high tissue P_{O_2} may be important to sustain exercise performance in these active piscivores.

As in other teleosts, especially those in the derived group of perciformes, Hb-O_2 binding in white seabass was highly pH sensitive. An increase in P_{CO_2} from arterial levels (0.3 kPa) to severe hypercapnia (2.5 kPa), caused a significant right-shift of the OEC (Fig. 1) via the Bohr effect, increasing P_{50} to 11.8 ± 0.3 kPa. When considering the corresponding changes in pH_e (from 8.1 to 7.2 over the range of tested P_{CO_2}; Supplemental Fig. S2*A*), the Bohr coefficient in white seabass was −0.92, and slightly higher, at −1.13, when considering the changes in RBC pH_i (from 7.7 to 7.0; Supplemental Fig. S2*B*). Again, these Hb-O_2 binding characteristics resemble closely those of rainbow trout, where P_{50} increased to 10 kPa during acidification (at 2 kPa P_{CO_2}), yielding a Bohr coefficient (relative to pH_e) of −0.87 (58). A normoxic increase in P_{CO_2} caused a significant reduction in Hb-O_2 saturation via the Root effect, and at P_{CO_2} above 3 kPa the O_2-carrying capacity of white seabass Hb was reduced by 52.4 ± 1.8% (DMSO treatment; Fig. 6*B*). These results are in line with those of other teleosts, such as rainbow trout (∼55%), tench (*Tinca tinca*; ∼50%), and the European perch (*Perca fluviatilis*; ∼70%), while also revealing some interspecific differences in the magnitude of the Root effect (42).

The Root effect is part of a specialized system of O_2 supply to the eye and the swim bladder of teleosts, where blood is acidified in a counter-current exchanger (the *rete mirabile*) to produce high P_{O_2} that bridge the large diffusion distances to the avascular retina of teleosts and inflate the swim bladder against large hydrostatic pressures (62). In the course of teleost evolution, there may have been numerous secondary losses of the choroid and swim bladder *retia* (24, 63). An ancestral state reconstruction found 23 independent losses of the choroid *rete*; however, none on the teleost branch leading up to the Sciaenidae, which include the white seabass (64). In addition, all of the five independent losses of the choroid *rete* have coincided with a reduction of the Root effect below 40% (24, 65). Thus, the large Root effect of white seabass is consistent with the presence of a choroid *rete* and likely critical for maintaining a high ocular P_{O_2} that facilitates visual acuity (15). Finally, the high pH sensitivity of Root-effect Hbs may enhance O_2 delivery to all tissues of teleosts including the swimming muscles (58, 66–68). Therefore, in white seabass the Root effect may generally be

important to support their ecological functions as highly active, visual predators.

Functional Characterization of β-NHE Activity

Adrenergic stimulation of white seabass RBCs with ISO caused a ~25% volume increase during the 60-min tonometry trials, whereas no changes in RBC volume were detected in DMSO-treated cells. The swelling response was corroborated by a significant reduction in MCHC and by visually confirming the increase in cell volume under a microscope, and these results closely match previous reports of RBC swelling after adrenergic stimulation in other teleosts (23, 69, 70). In addition, the ISO-induced swelling was abolished by the inhibition of NHEs in RBCs treated with ISO + Am, providing additional pharmacological support for the presence of a RBC β-NHE in white seabass. In ISO-treated RBCs, but not those treated with DMSO or ISO + Am, we observed a decrease in pH_e, which is the direct result of H^+ excretion by NHE activity. Corresponding changes in RBC pH_i are typically smaller because of the higher buffer capacity of the intracellular space ($pH_i = 0.67 \pm 0.07 \times pH_e$; Fig. 1), and the additional freeze-thaw steps and plasma removal may increase the variability of these measurements. Consequently, we were not able to resolve significant treatment effects on RBC pH_i, but a non-significant trend may point toward a small difference in RBC pH_i between ISO- and DMSO-treated RBCs ($P = 0.081$; Fig. 2*D*). Another interesting observation in these RBC swelling trials was the changes in cell morphology due to adrenergic stimulation. The increase in cell volume was largely due to an expansion along the *z*-axis of the cells, whereas the dimensions in the *x*-*y*-axis apparently remained unaffected. The nucleated RBCs of nonmammalian vertebrates, including fish, have a marginal band, a structural component of their cytoskeleton formed by strands of α-tubulin that maintains their elliptical shape in the face of shear and osmotic disturbances (71). The stiffness of this marginal band (72) may be a major impediment to swelling along the *x*-*y*-axis forcing the cells to widen in the *z*-direction.

The adrenergic activation of RBC β-NHEs results in a left-shift of the OEC by raising RBC pH_i above the equilibrium condition and this increases the arterial O_2-carrying capacity during a stress response (21). In the present study, we quantified the protective effect of β-NHE activation on Hb-O_2 saturation in white seabass under environmentally relevant levels of hypercapnia and hypoxia. As expected, Hb-O_2 saturation decreased significantly due to the Root effect, when P_{CO_2} was increased from 0.3 to 3 kPa (Fig. 5). However, adrenergic stimulation of the RBCs with ISO significantly delayed the reduction in Hb-O_2 saturation to higher EC_{50} P_{CO_2} that were 1.08 ± 0.06 kPa in ISO compared with 0.85 ± 0.06 kPa in DMSO-treated blood (Fig. 6*A*). In ISO + Am-treated RBC, the EC_{50} P_{CO_2} decreased significantly to 0.91 ± 0.06%, compared with ISO-treated cells, corroborating the involvement of the RBC β-NHE in the response. However, the EC_{50} P_{CO_2} of ISO + Am-treated RBCs was still significantly higher compared with DMSO controls, perhaps indicating that 1 mM amiloride did not lead to a full inhibition of the β-NHE under the tested conditions, or that other, amiloride insensitive transporters, play a role in elevating RBC pH_i after adrenergic stimulation.

Although β-NHE activity shifted the reduction in Hb-O_2 saturation to a higher P_{CO_2}, the magnitude of the Root effect was not affected by adrenergic stimulation (Fig. 6*B*). No significant differences were observed in Max. ΔHb-O_2 sat. in any of the tested treatments and therefore, a severe acidosis generated by high P_{CO_2} can overwhelm the physiological capacity of the β-NHE to protect RBC pH_i. The H^+ extrusion by the β-NHE is secondarily active and driven by the transmembrane Na^+ gradient created by the RBC Na^+-K^+-ATPase (NKA). Although both NKA activity (73) and the RBC rate of O_2 consumption ($\dot{M}O_2$) increase after adrenergic stimulation (74), it is possible that the capacity of the NKA to maintain the larger Na^+ gradients required to compensate for a greater reduction in pH_i is limited, as could be the availability of ATP to fuel the exchange. In addition, H^+ that are extruded by the β-NHE will react with HCO_3^- in the plasma to form CO_2 that can, once again, diffuse into the cells. This re-acidification of the cells via CO_2 is part of the Jacobs–Stewart cycle and typically rate limited by the formation of CO_2 in the plasma of teleosts (75). However, as pH_e decreases, the pool of plasma H_2CO_3 becomes larger, accelerating the Jacobs–Stewart cycle and the re-acidification of the cells (76), which may explain, in part, why β-NHE activity is ineffective at very high P_{CO_2}.

The benefit of β-NHE activity on Hb-O_2 saturation was nonlinear over the range of P_{CO_2} tested, and in normoxia the bell-shaped response had a maximum at ~1 kPa P_{CO_2} (Fig. 7*A*). The observed relationship is likely dependent on the sigmoidal shape of the OEC, where a left-shift due to β-NHE activity has only marginal effects when Hb-O_2 saturation is high and the curve is flat (77). In addition, β-NHE activity in many teleosts is stimulated by high intracellular $[H^+]$ and inhibited by high extracellular $[H^+]$ as pH_e decreases, resulting in a bell-shaped relationship between β-NHE activity and pH (78). The ecological implications are noteworthy, as the protective effect of β-NHE activity on Hb-O_2 binding is greatest over the range of P_{CO_2} that wild white seabass currently experience during severe red-tide or upwelling events. The increase in Hb-O_2 saturation at these P_{CO_2} is ~8%, and the effect can be harnessed continuously with every pass of the RBCs through the gills. Everything else being equal, an increase in arterial O_2 content can sustain a proportionally higher $\dot{M}O_2$, increasing the scope for activity or reducing the requirements for anaerobic pathways of ATP production that can lead to a toxic accumulation of metabolic by-products, such as lactate and H^+. Thus, for fish that experience a potentially life-threatening surge in P_{CO_2}, an 8% increase in arterial O_2 content could make the difference between escaping into less-noxious waters or perishing in the attempt.

In the hypoxic trials, DMSO-treated blood at arterial P_{CO_2} (0.3 kPa) had a Hb-O_2 saturation of 55.0 ± 3.3% (Fig. 5), which was close to the target value around Hb P_{50}. As in normoxia, an increase in P_{CO_2} caused a significant reduction in Hb-O_2 saturation, indicating the presence of a Root effect in hypoxia, which further decreased Hb-O_2 saturation, even below the level of the maximal normoxic Root effect. Consequently, H^+ binding to Hb must occur over nearly the entire range of the OEC, which stands in contrast to previous findings in rainbow trout where the Bohr effect and H^+ binding to Hb occurred largely in the upper half of the OEC (79, 80). The possibility of interspecific differences in the interaction between Hb-O_2

and H^+ binding cannot be resolved from the present data. However, it seems more likely that the kinetics of H^+ binding that induce the Bohr effect are different from those of the Root effect, which is supported by previous work indicating different molecular mechanisms for the two effects (81, 82). The interacting kinetics of O_2 and H^+ binding to the Root effect Hbs of teleosts remain a worthwhile avenue for future research and studying a broader range of environmental and metabolic scenarios, in more species, may strengthen the important ecological implications of the present work.

As in normoxic blood, adrenergic activation of the β-NHE in hypoxia increased Hb-O_2 saturation during a hypercapnic acidosis. This protective effect of the β-NHE was reflected in a significantly higher EC_{50} P_{CO_2} in ISO- compared with DMSO- or ISO + Am-treated RBCs (Fig. 6*A*). A significant main effect of O_2 on EC_{50} P_{CO_2} would indicate that in hypoxic blood a lower P_{CO_2} is required to desaturate Hb, compared with normoxic blood. However, this parameter estimate is influenced by the combined effects of P_{O_2} and P_{CO_2} on Hb-O_2 saturation (by taking into account the full scale from 0% to 100%), which is not easily untangled statistically. Importantly, there was no drug × O_2 interaction, indicating that the effect of the drugs was similar under normoxia and hypoxia, highlighting the benefit of β-NHE activation under both conditions.

As in normoxia, the benefit of β-NHE activation on Hb-O_2 saturation in hypoxia was nonlinear over the tested range of P_{CO_2} (Fig. 7*B*). β-NHE activation in hypoxic blood caused the largest increase in Hb-O_2 saturation at arterial P_{CO_2} (0.3 kPa) and the benefits decreased markedly toward higher levels of hypercapnia; likely due to the flattening of the OEC at low Hb-O_2 saturations and perhaps some inhibition of the transporter by the increasing extracellular [H^+]. The effect of β-NHE activity on Hb-O_2 binding was larger in hypoxia compared with normoxia, and at 0.3 kPa P_{CO_2} Hb-O_2 saturation increased by 11 ± 0.4%. This effect is even greater when considering that the available O_2-carrying capacity is lower in hypoxia and when expressed relative to the available Hb-O_2 saturation (55% in DMSO-treated blood), the relative benefit of β-NHE activity was 19.2 ± 0.0%. Many teleost β-NHEs are O_2 sensitive (83), and the larger effects of β-NHE activity on Hb-O_2 saturation in hypoxia may be related to a partial inhibition of the transporter in normoxia; whereas the effect appears to be less severe in white seabass compared with other species (30, 70, 84). The nearly 20% increase in Hb-O_2 saturation due to β-NHE activity is of great ecological significance and could be a principal pathway to safeguard arterial O_2 transport and facilitate hypoxic survival of white seabass in the wild. However, the present data also indicate a diminishing benefit of the β-NHE response when P_{CO_2} increases, revealing a potential vulnerability of white seabass to the combined stressors of hypoxia and hypercapnia; surviving these conditions likely requires additional behavioral and metabolic adjustments, which are yet to be determined.

Perspectives and Significance

The present study provides a thorough characterization of the Hb-O_2 binding system of white seabass and its modulation by the cellular mechanisms in RBCs that respond to adrenergic stimulation. Super-resolution microscopy detected an adrenergically induced translocation of β-NHE protein from vesicle-like structures within the RBC into the plasma membrane. This novel cellular pathway is consistent with previous observations and may be a general mechanism by which vertebrate RBCs regulate membrane transporter activity and that deserves further investigation. We corroborated these microscopy results with a thorough molecular, phylogenetic, and functional characterization of β-NHE activity in white seabass within a physiologically relevant context. The activation of RBC β-NHEs provided significant protection of Hb-O_2 binding during hypercapnic acidification with maximal benefits around the ecologically relevant level of ~1 kPa P_{CO_2}. Large benefits of β-NHE activation were also observed in hypoxia, however, with a greater sensitivity to increases in P_{CO_2}. Combined, these data indicate that adrenergic signaling and RBC function play a critical role in modulating the O_2-binding characteristics of the pH-sensitive Hbs in white seabass and are likely part of a suite of physiological responses that determines their hypoxia and hypercapnia tolerance. Finally, these results also highlight a potential vulnerability of white seabass to combinations of these stressors and further research is needed to study the implications for wild fish conservation along the steadily warming and eutrophicated California coast and in high-density aquaculture.

SUPPLEMENTAL DATA

Supplemental Tables S1 and S2, Supplemental Figs. S1–S7, and Supplemental Movies S1 and S2: https://doi.org/10.6084/m9.figshare.15505941.v1.

All raw data and R source code: https://doi.org/10.6084/m9.figshare.15505965.v1.

Sequence data is available through NCBI (see detailed accession numbers in manuscript and supplement Table S1).

ACKNOWLEDGMENTS

We thank Mark Drawbridge and the Hubbs SeaWorld Research Institute (HSWRI) for generously providing the white seabass and Phil Zerofski, Ashleigh Palinkas, Garfield Kwan, and Daniel Jio for help with animal care.

GRANTS

T. S. Harter and this study were supported by a National Science Foundation (NSF) Grant to M. Tresguerres (Award No. 1754994), and A. M. Clifford was supported by a SIO Postdoctoral Scholar Fellowship.

DISCLOSURES

No conflicts of interest, financial or otherwise, are declared by the authors.

AUTHOR CONTRIBUTIONS

T.S.H. conceived and designed research; T.S.H. and A.M.C. performed experiments; T.S.H. and A.M.C. analyzed data; T.S.H., A.M.C., and M.T. interpreted results of experiments; T.S.H. and A.M.C. prepared figures; T.S.H. drafted manuscript; T.S.H., A.M.C., and M.T. edited and revised manuscript; T.S.H., A.M.C., and M.T. approved final version of manuscript.

REFERENCES

1. **Frieder CA**, **Nam SH**, **Martz TR**, **Levin LA.** High temporal and spatial variability of dissolved oxygen and pH in a nearshore California kelp forest. *Biogeosciences* 9: 3917–3930, 2012. doi:10.5194/bg-9-3917-2012.
2. **Van Dolah FM.** Marine algal toxins: origins, health effects, and their increased occurrence. *Environ Health Perspect* 108, Suppl 1: 133–141, 2000. doi:10.1289/ehp.00108s1133.
3. **Diaz RJ**, **Rosenberg R.** Spreading dead zones and consequences for marine ecosystems. *Science* 321: 926–929, 2008. doi:10.1126/science.1156401.
4. **Harley CDG**, **Hughes AR**, **Hultgren KM**, **Miner BG**, **Sorte CJB**, **Thornber CS**, **Rodriguez LF**, **Tomanek L**, **Williams SL.** The impacts of climate change in coastal marine systems. *Ecol Lett* 9: 228–241, 2006, [Erratum in *Ecol Lett* 9: 500, 2006]. doi:10.1111/j.1461-0248.2005.00871.x.
5. **Clements SC**, **Takeshita Y**, **Dickson A**, **Martz T**, **Smith JE.** *Scripps Ocean Acidification Real-time (SOAR) Dataset*. Scripps Institution of Oceanography, La Jolla, CA. 2020.
6. **Boutilier RG**, **Heming TA**, **Iwama GK.** Physicochemical parameters for use in fish respiratory physiology. In: *Fish Physiology*, edited by Hoar WS, Randall DJ. New York: Academic Press, 1984, p. 403–426.
7. **Lewis E**, **Wallace DWR.** Program Developed for CO_2 System Calculations. ORNL/CDIAC-105. Oak Ridge, TN: Oak Ridge Natl. Lab, Carbon Dioxide Information Analysis Centre, 1998.
8. **Vaquer-Sunyer R**, **Duarte CM.** Thresholds of hypoxia for marine biodiversity. *Proc Natl Acad Sci USA* 105: 15452–15457, 2008. doi:10.1073/pnas.0803833105.
9. **Hughes GM.** Respiratory responses to hypoxia in fish. *Am Zool* 13: 475–489, 1973. doi:10.1093/icb/13.2.475.
10. **Jensen FB**, **Weber RE.** Respiratory properties of tench blood and hemoglobin. Adaptation to hypoxic-hypercapnic water. *Mol Physiol* 2: 235–250, 1982.
11. **Mandic M**, **Todgham AE**, **Richards JG.** Mechanisms and evolution of hypoxia tolerance in fish. *Proc Biol Sci* 276: 735–744, 2009. doi:10.1098/rspb.2008.1235.
12. **Bohr C**, **Hasselbalch K**, **Krogh A.** About a new biological relation of high importance that the blood carbonic acid tension exercises on its oxygen binding. *Skand Arch Physiol* 16: 402–412, 1904.
13. **Root RW.** The respiratory function of the blood of marine fishes. *Biol Bull* 61: 427–456, 1931. doi:10.2307/1536959.
14. **Scholander PF**, **Van Dam L.** Secretion of gases against high pressures in the swimbladder of deep sea fishes. I. Oxygen dissociation in blood. *Biol Bull* 107: 247–259, 1954. doi:10.2307/1538611.
15. **Damsgaard C**, **Lauridsen H**, **Harter TS**, **Kwan GT**, **Thomsen JS**, **Funder AM**, **Supuran CT**, **Tresguerres M**, **Matthews PG**, **Brauner CJ.** A novel acidification mechanism for greatly enhanced oxygen supply to the fish retina. *ELife* 9: e58995, 2020. doi:10.7554/eLife.58995.
16. **Pelster B.** Buoyancy at depth. In: *Fish Physiology*, edited by Randall D, Farrell A. New York: Academic Press, 1997, p. 195–238.
17. **Wittenberg JB**, **Wittenberg BA.** Active secretion of oxygen into the eye of fish. *Nature* 194: 106–107, 1962. doi:10.1038/194106a0.
18. **Randall DJ**, **Perry SF.** Catecholamines. In: *Fish Physiology*, edited by Hoar WS, Randall DJ, Farrell AP. New York: Academic Press, 1992, p. 255–300.
19. **Tetens V**, **Lykkeboe G**, **Christensen NJ.** Potency of adrenaline and noradrenaline for b-adrenergic proton extrusion from red cells of rainbow trout, *Salmo gairdneri*. *J Exp Biol* 134: 267–280, 1988. doi:10.1242/jeb.134.1.267.
20. **Mahé Y**, **Garcia-Romeu F**, **Motais R.** Inhibition by amiloride of both adenylate-cyclase activity and the Na^+/H^+ antiporter in fish erythrocytes. *Eur J Pharmacol* 116: 199–206, 1985. doi:10.1016/0014-2999(85)90154-2.
21. **Nikinmaa M.** Membrane transport and control of hemoglobin-oxygen affinity in nucleated erythrocytes. *Physiol Rev* 72: 301–321, 1992. doi:10.1152/physrev.1992.72.2.301.
22. **Rummer JL**, **Roshan-Moniri M**, **Balfry SK**, **Brauner CJ.** Use it or lose it? Sablefish, *Anoplopoma fimbria*, a species representing a fifth teleostean group where the βNHE associated with the red blood cell adrenergic stress response has been secondarily lost. *J Exp Biol* 213: 1503–1512, 2010. doi:10.1242/jeb.038844.
23. **Shu JJ**, **Harter TS**, **Morrison PR**, **Brauner CJ.** Enhanced hemoglobin-oxygen unloading in migratory salmonids. *J Comp Physiol B* 188:409–411, 2018. doi:10.1007/s00360-017-1139-9.
24. **Berenbrink M**, **Koldkjaer P**, **Kepp O**, **Cossins AR.** Evolution of oxygen secretion in fishes and the emergence of a complex physiological system. *Science* 307: 1752–1757, 2005. doi:10.1126/science.1107793.
25. **Montgomery DW**, **Simpson SD**, **Engelhard GH**, **Birchenough SNR**, **Wilson RW.** Rising CO_2 enhances hypoxia tolerance in a marine fish. *Sci Rep* 9: 15152, 2019. doi:10.1038/s41598-019-51572-4.
26. **Caldwell S**, **Rummer JL**, **Brauner CJ.** Blood sampling techniques and storage duration: effects on the presence and magnitude of the red blood cell beta-adrenergic response in rainbow trout (*Oncorhynchus mykiss*). *Comp Biochem Physiol A Mol Integr Physiol* 144: 188–195, 2006. doi:10.1016/j.cbpa.2006.02.029.
27. **Brauner CJ**, **Thorarensen H**, **Gallaugher P**, **Farrell AP**, **Randall DJ.** CO_2 transport and excretion in rainbow trout (*Oncorhynchus mykiss*) during graded sustained exercise. *Resp Physiol* 119: 69–82, 2000. doi:10.1016/S0034-5687(99)00091-2.
28. **van Kampen EJ**, **Zijlstra WG.** Spectrophotometry of hemoglobin and hemoglobin derivatives. In: *Advances in Clinical Chemistry*, edited by Latner AL, Schwartz MK. New York: Academic, 1983, p. 199–257.
29. **Zeidler R**, **Kim HD.** Preferential hemolysis of postnatal calf red cells induced by internal alkalinization. *J Gen Physiol* 70: 385–401, 1977. doi:10.1085/jgp.70.3.385.
30. **Motais R**, **Garcia-Romeu F**, **Borgese F.** The control of Na^+/H^+ exchange by molecular oxygen in trout erythrocytes. A possible role of hemoglobin as a transducer. *J Gen Physiol* 90: 197–207, 1987. doi:10.1085/jgp.90.2.197.
31. **Salama A**, **Nikinmaa M.** Species differences in the adrenergic responses of fish red cells: studies on whitefish, pikeperch, trout and carp. *Fish Physiol Biochem* 6: 167–173, 1989. doi:10.1007/BF01874773.
32. **Borgese F**, **Sardet C**, **Cappadoro M**, **Pouyssegur J**, **Motais R.** Cloning and expression of a cAMP-activated Na^+/H^+ exchanger: evidence that the cytoplasmic domain mediates hormonal regulation. *Proc Natl Acad Sci USA* 89: 6765–6769, 1992. doi:10.1073/pnas.89.15.6765.
33. **Clifford AM**, **Weinrauch AM**, **Edwards SL**, **Wilkie MP**, **Goss GG.** Flexible ammonia handling strategies using both cutaneous and branchial epithelia in the highly ammonia-tolerant Pacific hagfish. *Am J Physiol Regul Integr Comp Physiol* 313: R78–R90, 2017. doi:10.1152/ajpregu.00351.2016.
34. **Chen S**, **Zhou Y**, **Chen Y**, **Gu J.** fastp: an ultra-fast all-in-one FASTQ preprocessor. *Bioinformatics* 34: i884–i890, 2018. doi:10.1093/bioinformatics/bty560.
35. **Grabherr MG**, **Haas BJ**, **Yassour M**, **Levin JZ**, **Thompson DA**, **Amit I**, **Adiconis X**, **Fan L**, **Raychowdhury R**, **Zeng Q**, **Chen Z**, **Mauceli E**, **Hacohen N**, **Gnirke A**, **Rhind N**, **di Palma F**, **Birren BW**, **Nusbaum C**, **Lindblad-Toh K**, **Friedman N**, **Regev A.** Full-length transcriptome assembly from RNA-Seq data without a reference genome. *Nat Biotechnol* 29: 644–652, 2011. doi:10.1038/nbt.1883.
36. **Castresana J.** Selection of conserved blocks from multiple alignments for their use in phylogenetic analysis. *Mol Biol Evol* 17: 540–552, 2000. doi:10.1093/oxfordjournals.molbev.a026334.
37. **Talavera G**, **Castresana J.** Improvement of phylogenies after removing divergent and ambiguously aligned blocks from protein sequence alignments. *Syst Biol* 56: 564–577, 2007. doi:10.1080/10635150701472164.
38. **Miller MA**, **Pfeiffer W**, **Schwartz T.** Creating the CIPRES science gateway for inference of large phylogenetic trees. *Gateway Computing Environments Workshop (GCE)*. New Orleans, LA, 2010, p. 1–8.
39. **Le SQ**, **Gascuel O.** An improved general amino acid replacement matrix. *Mol Biol Evol* 25: 1307–1320, 2008. doi:10.1093/molbev/msn067.
40. **Kozak M.** An analysis of 5′-noncoding sequences from 699 vertebrate messenger RNAs. *Nucleic Acids Res* 15: 8125–8148, 1987. doi:10.1093/nar/15.20.8125.
41. **Nishikawa T**, **Ota T**, **Isogai T.** Prediction whether a human cDNA sequence contains initiation codon by combining statistical

information and similarity with protein sequences. *Bioinformatics* 16: 960–967, 2000 [Erratum in *Bioinformatics* 17: 290, 2001]. doi:10.1093/bioinformatics/16.11.960.

42. **Berenbrink M**, **Koldkjær P**, **Hannah Wright E**, **Kepp O**, **José da Silva A.** Magnitude of the Root effect in red blood cells and haemoglobin solutions of fishes: a tribute to August Krogh. *Acta Physiol* 202: 583–592, 2011. doi:10.1111/j.1748-1716.2010.02243.x.
43. **Wood CM**, **McDonald DG**, **McMahon BR.** The influence of experimental anemia on blood acid-base regulation *in vivo* and *in vitro* in the starry flounder (*Platichthys stellatus*) and the rainbow trout (*Salmo gairdneri*). *J Exp Biol* 96: 221–237, 1982. doi:10.1242/jeb.96.1.221.
44. **Dunn C**, **O'Dowd A**, **Randall RE.** Fine mapping of the binding sites of monoclonal antibodies raised against the Pk tag. *J Immunol Methods* 224: 141–150, 1999. doi:10.1016/s0022-1759(99)00017-4.
45. **Parks SK**, **Tresguerres M**, **Goss GG.** Blood and gill responses to HCl infusions in the Pacific hagfish (*Eptatretus stoutii*). *Can J Zool* 85: 855–862, 2007. doi:10.1139/Z07-068.
46. **Lawrence SP**, **Holman GD**, **Koumanov F.** Translocation of the Na^+/H^+ exchanger 1 (NHE1) in cardiomyocyte responses to insulin and energy-status signalling. *Biochem J* 432: 515–523, 2010. doi:10.1042/BJ20100717.
47. **Gens JS**, **Du H**, **Tackett L**, **Kong S-S**, **Chu S**, **Montrose MH.** Different ionic conditions prompt NHE2 and NHE3 translocation to the plasma membrane. *Biochim Biophys Acta* 1768: 1023–1035, 2007. doi:10.1016/j.bbamem.2007.01.003.
48. **Zhao H**, **Shiue H**, **Palkon S**, **Wang Y**, **Cullinan P**, **Burkhardt JK**, **Musch MW**, **Chang EB**, **Turner JR.** Ezrin regulates NHE3 translocation and activation after Na^+-glucose cotransport. *Proc Natl Acad Sci USA* 101: 9485–9490, 2004. doi:10.1073/pnas.0308400101.
49. **Reid SD**, **Perry SF.** Quantification of presumptive Na^+/H^+ antiporters of the erythrocytes of trout and eel. *Fish Physiol Biochem* 12: 455–463, 1994. doi:10.1007/BF00004448.
50. **Pedersen SF**, **King SA**, **Rigor RR**, **Zhuang Z**, **Warren JM**, **Cala PM.** Molecular cloning of NHE1 from winter flounder RBCs: activation by osmotic shrinkage, cAMP, and calyculin A. *Am J Physiol Cell Physiol* 284: C1561–C1576, 2003. doi:10.1152/ajpcell.00562.2002.
51. **Landau M**, **Herz K**, **Padan E**, **Ben-Tal N.** Model structure of the Na^+/H^+ exchanger 1 (NHE1): functional and clinical implications. *J Biol Chem* 282: 37854–37863, 2007. doi:10.1074/jbc.M705460200.
52. **Lee BLLL**, **Sykes BDSD**, **Fliegel LF.** Structural analysis of the Na^+/H^+ exchanger isoform 1 (NHE1) using the divide and conquer approach. *Biochem Cell Biol* 89: 189–199, 2011. doi:10.1139/O10-140.
53. **Chen XL**, **Zhang B**, **Chng YR**, **Ong JLY**, **Chew SF**, **Wong WP**, **Lam SH**, **Ip YK.** Na^+/H^+ exchanger 3 is expressed in two distinct types of ionocyte, and probably augments ammonia excretion in one of them, in the gills of the climbing perch exposed to seawater. *Front Physiol* 8: 880, 2017. doi:10.3389/fphys.2017.00880.
54. **Blair S**, **Li X**, **Dutta D**, **Chamot D**, **Fliegel L**, **Goss G.** Rainbow trout (*Oncorhynchus mykiss*) Na^+/H^+ exchangers tNhe3a and tNhe3b display unique inhibitory profiles dissimilar from mammalian NHE isoforms. *Int J Mol Sci* 22: 2205, 2021. doi:10.3390/ijms22042205.
55. **Mairbäurl H.** Red blood cell function in hypoxia at altitude and exercise. *Int J Sports Med* 15: 51–63, 1994. doi:10.1055/s-2007-1021020.
56. **Tenney SM.** Hypoxia and the brain: functional significance of differences in mammalian hemoglobin affinity for oxygen. In: *Proceeding of the 9th International Hypoxia Symposium*, edited by Sutton JR, Houston CS, Coates G. Lake Louise, Canada: Queen City Printers, Burlington, Vt., 1995, p. 57–68.
57. **Brauner CJ**, **Wang T**, **Val AL**, **Jensen FB.** Non-linear release of Bohr protons with haemoglobin-oxygenation in the blood of two teleost fishes; carp (*Cyprinus carpio*) and tambaqui (*Colossoma macropomum*). *Fish Physiol Biochem* 24: 97–104, 2001. doi:10.1023/A:1011944407938.
58. **Rummer JL**, **Brauner CJ.** Root effect haemoglobins in fish may greatly enhance general oxygen delivery relative to other vertebrates. *PloS One* 10: e0139477, 2015. doi:10.1371/journal.pone.0139477.
59. **Wells RMG.** Hemoglobin physiology in vertebrate animals: a cautionary approach to adaptationist thinking. In: *Advances in Comparative and Environmental Physiology: Vertebrate Gas Exchange from Environment to Cell*, edited by Boutilier RG. Berlin: Springer, 1990, p. 143–161.
60. **Brauner CJ**, **Wang T.** The optimal oxygen equilibrium curve: a comparison between environmental hypoxia and anemia. *Am Zool* 37: 101–108, 1997. doi:10.1093/icb/37.1.101.
61. **Mairbäurl H**, **Weber RE.** Oxygen transport by hemoglobin. *Compr Physiol* 2: 1463–1489, 2012. doi:10.1002/cphy.c080113.
62. **Pelster B**, **Randall DJ.** Physiology of the root effect. In: *Fish Physiology*, edited by Perry SF, Tufts BL. New York: Academic Press, 1998, p. 113–140.
63. **Wittenberg JB**, **Haedrich RL.** Choroid *rete mirabile* of fish eye. II. Distribution and relation to pseudobranch and to swimbladder *rete mirabile*. *Biol Bull* 146: 137–156, 1974. doi:10.2307/1540403.
64. **Damsgaard C**, **Lauridsen H**, **Funder AM**, **Thomsen JS**, **Desvignes T**, **Crossley DA 2nd**, **Møller PR**, **Huong DT**, **Phuong NT**, **Detrich HW 3rd**, **Brüel A**, **Wilkens H**, **Warrant E**, **Wang T**, **Nyengaard JR**, **Berenbrink M**, **Bayley M.** Retinal oxygen supply shaped the functional evolution of the vertebrate eye. *ELife* 8: e52153, 2019. doi:10.7554/eLife.52153.
65. **Berenbrink M.** Historical reconstructions of evolving physiological complexity: O_2 secretion in the eye and swimbladder of fishes. *J Exp Biol* 210: 1641–1652, 2007. doi:10.1242/jeb.003319.
66. **Harter TS**, **Zanuzzo FS**, **Supuran CT**, **Gamperl AK**, **Brauner CJ.** Functional support for a novel mechanism that enhances tissue oxygen extraction in a teleost fish. *Proc Biol Sci* 286: 20190339, 2019. doi:10.1098/rspb.2019.0339.
67. **Rummer JL**, **McKenzie DJ**, **Innocenti A**, **Supuran CT**, **Brauner CJ.** Root effect hemoglobin may have evolved to enhance general tissue oxygen delivery. *Science* 340: 1327–1329, 2013. doi:10.1126/science.1233692.
68. **Randall DJ**, **Rummer JL**, **Wilson JM**, **Wang S**, **Brauner CJ.** A unique mode of tissue oxygenation and the adaptive radiation of teleost fishes. *J Exp Biol* 217: 1205–1214, 2014. doi:10.1242/jeb.093526.
69. **Nikinmaa M**, **Huestis WH.** Adrenergic swelling of nucleated erythrocytes—cellular mechanisms in a bird, domestic goose, and 2 teleosts, striped bass and rainbow trout. *J Exp Biol* 113: 215–224, 1984. doi:10.1242/jeb.113.1.215.
70. **Weaver YR**, **Kiessling K**, **Cossins AR.** Responses of the Na^+/H^+ exchanger of European flounder red blood cells to hypertonic, beta-adrenergic and acidotic stimuli. *J Exp Biol* 202: 21–32, 1999. doi:10.1242/jeb.202.1.21.
71. **Joseph-Silverstein J**, **Cohen WD.** The cytoskeletal system of nucleated erythrocytes. III. Marginal band function in mature cells. *J Cell Biol* 98: 2118–2125, 1984. doi:10.1083/jcb.98.6.2118.
72. **Dmitrieff S**, **Alsina A**, **Mathur A**, **Nédélec FJ.** Balance of microtubule stiffness and cortical tension determines the size of blood cells with marginal band across species. *Proc Natl Acad Sci USA* 114: 4418–4423, 2017. doi:10.1073/pnas.1618041114.
73. **Bourne PK**, **Cossins AR.** On the instability of K^+ influx in erythrocytes of the rainbow trout, *Salmo gairdneri*, and the role of catecholamine hormones in maintaining *in vivo* influx activity. *J Exp Biol* 101: 93–104, 1982. doi:10.1242/jeb.101.1.93.
74. **Boutilier RG**, **Ferguson RA.** Nucleated red cell function: metabolism and pH regulation. *Can J Zool* 67: 2986–2993, 1989. doi:10.1139/z89-421.
75. **Jacobs MH**, **Stewart DR.** The role of carbonic anhydrase in certain ionic exchanges involving the erythrocyte. *J Gen Physiol* 25: 539–552, 1942. doi:10.1085/jgp.25.4.539.
76. **Motais R**, **Fievet B**, **Garcia-Romeu F**, **Thomas S.** Na^+-H^+ exchange and pH regulation in red blood cells: role of uncatalyzed $H_2CO_3^-$ dehydration. *Am J Physiol Cell Physiol* 256: C728–C735, 1989. doi:10.1152/ajpcell.1989.256.4.C728.
77. **Kobayashi M**, **Ishigaki K**, **Kobayashi M**, **Imai K.** Shape of the haemoglobin-oxygen equilibrium curve and oxygen transport efficiency. *Resp Physiol* 95: 321–328, 1994. doi:10.1016/0034-5687(94)90094-9.

78. **Borgese F**, **Garcia-Romeu F**, **Motais R.** Ion movements and volume changes induced by catecholamines in erythrocytes of rainbow trout: effect of pH. *J Physiol* 382: 145–157, 1987. doi:10.1113/jphysiol.1987.sp016360.
79. **Brauner CJ**, **Gilmour KM**, **Perry SF.** Effect of haemoglobin oxygenation on Bohr proton release and CO_2 excretion in the rainbow trout. *Resp Physiol* 106: 65–70, 1996. doi:10.1016/0034-5687(96)00061-8.
80. **Brauner CJ**, **Thorarensen H**, **Gallaugher P**, **Farrell AP**, **Randall DJ.** The interaction between O_2 and CO_2 exchange in rainbow trout during graded sustained exercise. *Resp Physiol* 119: 83–96, 2000. doi:10.1016/S0034-5687(99)00095-X.
81. **Brittain T.** The Root effect. *Comp Biochem Physiol B* 86: 473–481, 1987. doi:10.1016/0305-0491(87)90434-2.
82. **Perutz MF**, **Brunori M.** Stereochemistry of cooperative effects in fish and amphibian haemoglobins. *Nature* 299: 421–426, 1982. doi:10.1038/299421a0.
83. **Gibson J**, **Cossins A**, **Ellory J.** Oxygen-sensitive membrane transporters in vertebrate red cells. *J Exp Biol* 203: 1395–1407, 2000. doi:10.1242/jeb.203.9.1395.
84. **Salama A**, **Nikinmaa M.** The adrenergic responses of carp (*Cyprinus carpio*) red cells: effects of PO_2 and pH. *J Exp Biol* 136: 405–416, 1988. doi:10.1242/jeb.136.1.405.